CERN-PPE/95-61
May 9, 1995

EUROPEAN ORGANIZATION FOR NUCLEAR RESEARCH

Measurement of Hadronic Shower Punchthrough in Magnetic Field

RD5 Collaboration, CERN, Geneva, Switzerland

C. Albajar[13], M. Andlinger[22], A. Arefiev[14], C. Bacci[19], Gy. L. Bencze[4], R. Bergman[15], A. Bizzeti[8], C. Brouwer[2], R. Cardarelli[18], P. Casoli[16], S. Centro[16], F. Ceradini[19], E. Choumilov[14], D. Chrisman[5], G. Ciapetti[17], C. Civinini[8], D. Cline[5], R. D'Alessandro[8], M. Della Negra[7], E. Denes[4], A. Di Ciaccio[18], W. Dominik[23], H. Faissner[1], A. Ferrando[12], M.C. Fouz[12], W. Gorn[6], M. Górski[24], A. Hervé[7], A. Iglesias[12,a], M. Juntunen[10], V. Karimäki[10], R. Kinnunen[9], A. Kluge[22], Yu. Kolotaev[14], M. Konecki[23], A.C. König[15], J. Królikowski[23], F. Lacava[17], J.G. Layter[6], P. Le Coultre[25], C. Lyndon[11], A. Malinin[14], G. Margutti[17], R. Martinelli[16], L. Martinez-Laso[12], R. McNeil[11], A. Meneguzzo[16], M. Meschini[8], T. Moers[1], M. Mohammadi-Baarmand[20], A. Nisati[17], D. Orestano[17], K. Österberg[21], S. Otwinowski[5], E. Petrolo[17], M. Pimiä[10], V. Pojidaev[8], C. L. A. Pols[15], L. Pontecorvo[17], P. Porth[22], E. Radermacher[7], B. Razen[1], H. Reithler[1], R. Ribeiro[7], A. Rojkov[14], A. Sanjari[20], R. Santonico[18], P. Sartori[16], J. Shank[3], H. Schwarthoff[1], C. Seez[7,b], B.C. Shen[6], M. Szeptycka[24], F. Szoncso[22], H. Teykal[1], H. Tolsma[2], H. Tuchscherer[1,c], J. Tuominiemi[9], T. Tuuva[10], H. van der Graaf[2], S. Veneziano[17], M. Verzocchi[17], G. Vesztergombi[4], H. Wagner[1], G. Walzel[22], T. Wijnen[15], G.W. Wilson[6], G. Wrochna[7,24], C.-E. Wulz[22], L. Zanello[17], and P. Zotto[16,d]

Aachen[1], Amsterdam (NIKHEF-H)[2], Boston University[3], Budapest[4], UC Los Angeles[5], UC Riverside[6], CERN[7], Firenze[8], Helsinki[9], Helsinki(SEFT)[10], Louisiana State University[11], Madrid (CIEMAT)[12], Madrid (Universitad Autónoma)[13], Moscow[14], Nijmegen[15], Padova[16], Roma "La Sapienza"[17], Roma "Tor Vergata"[18], Roma "Terza Universitá"[19], SUNY at Stony Brook[20], Turku[21], Vienna (HEPHY)[22], Warsaw University[23], Institute for Nuclear Studies, Warsaw[24], Zürich[25]

Abstract

The total punchthrough probability of showers produced by negative pions, positive pions, positive kaons and protons, has been measured as a function of depth in an absorber in a magnetic field ranging from 0 to 3 Tesla. The incident particle momentum varied from 10 to 300 GeV/*c*. The lateral shower development and particle multiplicity at several absorber depths have been determined. The measurements are compared with the predictions of Monte Carlo simulation programs.

Submitted to Zeitschrift für Physik C

[a] Doctoral student from Univ. of Santiago de Compostela, Spain.
[b] Visitor from Imperial College, London, U.K.
[c] Now at Univ. of Alabama, USA.
[d] Now at Dipartmento di Fisica del Politecnico, Milano, Italy.

1 Introduction

The unprecedented design luminosity ($\mathcal{L} > 10^{34}\text{cm}^{-2}\text{s}^{-1}$) and center of mass energy ($\sqrt{s}$ = 14 TeV) planned for the Large Hadron Collider (LHC), extends considerably the mass range for the discovery of Higgs and SUSY particles, additional W and Z bosons, and other new particles. Single lepton and dilepton triggers are expected to play a crucial role in tagging the decay of these heavy particles. In this high rate environment, muons offer an advantage over electrons since the trigger decision can be made after a thick absorber where the particle flux is low.

The prompt muon rate at the LHC is expected to be very high and dominated at all transverse momentum values by muons from charm and bottom decays [1]. Sources of muon backgrounds in a typical collider detector are: uncorrelated neutrons and gammas coming from hadronic interactions in a very forward calorimeter, muons from π and K decays in a tracking volume in front of a calorimeter, and hadronic punchthrough. Hadronic punchthrough consists of two components: penetrating muons from π and K decays in the hadronic shower cascade and other charged particles (mainly soft hadrons and electrons) composing the unabsorbed remnant of the hadronic shower. Therefore, in this text when we speak of *punchthrough particles*, we mean punchthrough muons and all other particles exiting the calorimeter. Likewise, when we refer to *punchthrough muons*, we refer only to the muon component.

In the design of detectors for the LHC, it is important to understand the punchthrough contribution to the trigger rates. Furthermore, high particle rates in the muon measurement stations, due partly to hadronic punchthrough, can affect track segment reconstruction efficiency. Pattern recognition algorithms may fail to efficiently identify track segments if there are too many nearby tracks.

The RD5 collaboration at CERN [2] was formed to study topics related to muon detection at future hadron colliders. These topics included: measurement of the total punchthrough probability of hadronic showers [3], measurement of angular and momentum distributions of punchthrough muons [4] and study of the influence of a strong magnetic field on punchthrough particles. In addition, RD5 has conducted muon trigger studies, investigated the effect of electromagnetic secondaries on muon measurement [5] and tested various types of large area muon detectors. An overview of the RD5 experimental program can be found in [6].

In Sections 2 and 3 below, we describe the RD5 detector and the experimental method used to measure total punchthrough. In Section 4, the Monte Carlo simulation program is described. Next, in Section 5, we present the results of measurements of the total punchthrough probability of hadrons as a function of meters of iron equivalent for an absorber in a 3 T magnetic field, 1.5 T field and no field. The lateral distribution of shower particles and the shower particle multiplicity measured at two absorber depths are also presented. The effect of the magnetic field on these measured quantities is shown and the measurements are compared with the results of a Monte Carlo simulation. Finally, in Section 6, the results are summarized.

2 The RD5 detector

The RD5 experiment is located in the H2 beam of the CERN SPS North Area. The experimental set-up is shown in Fig. 1. The detector was designed to simulate a CMS-like detector [7], having tracking detectors, a calorimeter in a magnetic field and muon measurement stations in an iron return yoke. Each muon station consists of drift chambers and Resistive Plate Chambers (RPCs) [8]. The set-up includes two magnets, a superconducting magnet (M1), with a maximum 3 T field, and an iron toroidal magnet (M2) operated at 1.5 T. The magnet M1, which contains a tracking calorimeter (TRACAL), simulates the strong solenoidal field of CMS, while the magnet M2 simulates the CMS

return yoke. The magnet M2, which is used as an absorber, is constructed as a closed magnetic circuit, 1.8 to 2 m thick.

The tracking calorimeter, TRACAL, consists of stainless steel plates interleaved with Honeycomb Strip Chambers (HSC)[9]. Each chamber has an active area of 0.6×0.8 m^2, with 22 mm gaps between the absorbers. TRACAL was separated into two units. Between the first 13 HSC chambers, the absorbers (stainless steel plates 0.8×1.0 m^2) were 40 mm thick, thus totaling 12 times 0.25 nuclear interaction lengths, λ. The next 12 gaps between the HSC chambers were filled with plates, each 80 mm thick, totaling another 12 times 0.5λ. The total absorption power of TRACAL is therefore 9λ. In front of TRACAL, a lead brick wall, of about one interaction length (29 X_0), was installed to account for the absorption of an electromagnetic calorimeter.

Three muon measurement stations are installed in front of, inside and behind the magnet M2 (see Fig. 1). The muon drift chambers [10] are used for precise measurement of particle trajectories in the RD5 spectrometer. RPCs equipped with 30 mm read-out strips in both projections [11] are placed on either side of the drift chambers. The muon station 1, being just after TRACAL, is at a depth of 10 λ. The muon stations 2 and 3 are at depths of 21λ and 31λ, respectively.

The beam definition is provided by two multiwire proportional chambers (MWPCs: U1 and U3) and a silicon beam telescope.

The magnet M1 [12] is composed of two parallel superconducting coils without a yoke. In the RD5 coordinate system, the axis of the two coils is oriented along the z-direction, transverse to the beam direction. The beam is along the x-direction. In the region between the two coils, the magnetic field is oriented predominately in the z-direction. At the maximum field of 3 T, the radial component is less than 0.67 % in the region near the beam line. In Fig. 2, the magnitude of the magnetic field, $|B_z|$, is plotted as a function of x and z. TRACAL sits at the origin of the coordinate system and extends to ± 1.1 m in the x-direction and ± 0.4 m in the z-direction. One sees that the field strength varies significantly over the length of TRACAL, along the beam-line, falling to about 50% of its maximum value at ± 1.1 m. The bending power of M1 can be expressed as $\int \vec{B} \times d\vec{l}$, evaluated over the length of TRACAL and along the beam axis (-110 cm $\leq x \leq +110$ cm, $y = 0, z = 0$). The bending power of M1 evaluated over the length of TRACAL is 5.2 T·m. A uniform 4 T field in the barrel region of CMS will have a bending power of about 12 T·m.

Parts of the RD5 detector have been modified since the first run in 1991. Four new 2×2 m^2 planes of RPC chambers were added in the second and in the third muon measurement station, with one plane on either side of the drift chambers. Each plane is made of two RPCs with 30 mm wide read-out strips. All new detector planes are made of double-gap RPCs [13] that insure a better efficiency and a more precise timing. Furthermore, for the study of hadronic punchthrough, there needs to be an efficient veto against hits produced by off-time and halo muons. A veto wall, that covers the entire area of the muon drift chambers, was built with an array of RPCs and placed 1.2 m upstream of the magnet M1.

The RD5 trigger system (see also Fig. 1) consists of scintillators S1 and S5 for the beam definition and S4a-b for beam size determination. The system of counters S2 and S3, together with the RPC veto wall described above, form a veto system against beam halo particles. It is ensured that there are no other particles crossing the 4×4 m^2 area of the RPC wall within $\pm 2\mu$s around the triggering one.

Two trigger modes were used for the measurement of total punchthrough: a minimum bias trigger (MB) and a ten-lambda (10λ) trigger. The minimum bias trigger consisted of scintillators S1 and S5 in anti-coincidence with the veto system, thus flagging a single particle entering the detector. The 10λ trigger consisted of the minimum bias trigger with the additional requirement that there was at least one hit in the RPC counters in the muon station 1, at an absorber depth of 10λ.

A Cerenkov counter was used for running with positive pions, kaons and protons in order to

distinguish various kinds of particles.

3 The data sample and analysis method

During the 1991 run period, data were taken with negative muon and pion beams. The beam momenta were 30, 40, 50, 75, 100, 200 and 300 GeV/c. The muon data were used to characterize the muon contamination in the pion beam and for detector calibration. The results of the analysis of the 1991 data have been previously published [3].

In 1992 and 1993, the RD5 data set was expanded and also included negative pions of momentum 10 and 20 GeV/c as well as positive hadrons (π^+, K^+ and protons) of momentum 30 to 300 GeV/c. Data were also taken with the magnet M1 at full field (3 Tesla) and at half field.

We define the *total punchthrough probability* of hadronic showers at a given depth x as the ratio of the number of events with at least one hit in the detector at that depth x over the total number of events. This definition should be distinguished from the *integral punchthrough probability*, which is defined as the number of hits measured in a detector divided by the total number of events. The integral punchthrough probability is equal to the total punchthrough probability times the average number of hits per event.

An algorithm, which accounts for chamber efficiencies and noise levels, was developed in order to find the actual penetration depth of each punchthrough particle. For data taken with the MB trigger, the pion and kaon beams contained from 2 to 10% muon contamination, depending on beam momentum and particle type. The muon contamination comes from π or K decays upstream of the detector. Therefore, it was necessary to subtract this muon background off-line. The algorithm which determines the most probable punchthrough depth of each event and subtracts the muon background is described in detail in reference [3].

The efficiency of the RPCs in the veto wall was about 95%, thus not all halo muons were rejected. In addition there were some muons entering the detector at large angles outside of the area of the veto wall. An additional muon background comes from the presence of halo muons which occurred in coincidence with normal hadronic showers. These events are characterized by having a large hadronic shower in the calorimeter followed by a muon track reaching the muon station 3. Events were identified as halo and rejected from the analysis if the muon track did not point back to the calorimeter. For the π^- beam (depending on the beam momentum), 30% to 40% of all tracks reaching the muon station 3 did not point back to the calorimeter. For the π^+ beam the fraction was about 10%. These numbers were verified by visually scanning a sample of all events reaching the muon station 3 (100 events of each data set).

A further requirement is that only a single beam particle enters the calorimeter. For each trigger, all events with more than one track in MWPCs, U1 and U2, are excluded from the analysis. This requirement excludes particles which begin to shower upstream of the calorimeter.

During data taking, the 10λ trigger was used in order to increase measurement statistics at absorber depths greater than 10λ. For example, the number of events with particles reaching the muon station 3 (31λ) was increased by a factor 2 to 7 (depending on the total number of 10λ triggers recorded) over the statistics with the MB trigger alone. The correct trigger normalization for the data taken with the 10λ trigger, was found by counting the number of 10λ triggers which occur as a subset of the minimum bias triggers. After the results obtained with the 10λ trigger condition had been properly normalized, the two sets of results (MB and 10λ) were combined by a weighted average. The event statistics used in the present measurement of total punchthrough are presented in Tables 1 and 2, for both MB and 10λ trigger conditions.

Particle momentum [GeV/c]	Particle type			
	π^-	π^+	K^+	proton
	Event statistics, M1 field 0 T			
10	69000			
20	61000			
30	101000	86000		
50	77000			
100	103000	70000	39000	68000
200	35000			
300	36000	61000		30000
	Event statistics, M1 field 1.5 T			
30	83000			
100	77000	65000		
300	37000			
	Event statistics, M1 field 3 T			
10	59000			
20	83000			
30	85000	85000		
50	79000		90000	
100	53000	37000	52000	46000
200	50000			
300	40000	45000		43000

Table 1: Event statistics with minimum bias trigger (MB), used in the analysis to measure total punchthrough.

Particle momentum [GeV/c]	Particle type			
	π^-	π^+	K^+	proton
	Event statistics, M1 field 0 T			
10				
20	28000			
30	50000	53000		
50	44000			
100	52000	31000	11000	45000
200	14000			
300	13000	30000		20000
	Event statistics, M1 field 1.5 T			
30	42000			
100	27000	12000		
300	20000			
	Event statistics, M1 field 3 T			
10				
20				
30		43000		
50	32000		40000	
100	26000	20000	25000	31000
200	23000			
300	28000	16000		14000

Table 2: Event statistics collected with ten lambda trigger (10λ) used in the analysis to measure total punchthrough.

4 Description of Monte Carlo simulation

Simulations of the RD5 experiment have been performed for five different momenta of π^- beam and one momentum of K^+. A primary purpose of the simulation is to validate the GEANT code, so that confidence may be held in its predictions concerning detector designs that are based on this widely used simulation program. The detectors included in the simulation were TRACAL, the RPCs, and the muon drift chambers. Also included in the simulation were both magnets (M1 and M2), the lead brick in front of TRACAL and some concrete supports for the magnet M2. The simulation accounted for the 1.5 T field of M2 and two different field conditions of M1, 0 and 3 T.

GEANT version 3.21 [14] was used for the simulation. Hadronic interactions were treated with the hadronic shower generators GHEISHA [15] and FLUKA [16], for 10, 30, 50, 100 and 300 GeV/c negative pions, and GHEISHA, for 50 GeV/c positive kaons. The number of events generated ranged from 20,000 at 10 GeV/c to 3000 at 300 GeV/c.

Digitization of charged particle hits in detectors were simulated and written to a file in the same format as the real data; these data were then processed with the same analysis program used for the real data. The GEANT energy thresholds used were, 1 MeV for all types of particles in the absorbers, and 10 keV for electrons and gammas in the sensitive volumes of the detectors. The lower threshold in the sensitive volumes allowed photons to interact and produce low-energy electrons which could then be counted as hits. Further reducing these thresholds did not result in any significant changes in punchthrough distributions. The processes included in the simulation were pair production, bremsstrahlung, delta-ray production, photonuclear fission, photo-electric effect, Compton scattering, Rayleigh scattering, muon-nuclear interactions, multiple scattering, annihilation and decays. The beam spot was simulated as a gaussian distribution with a width consistent with the MWPC measurements.

5 Results

5.1 Total punchthrough probability of hadronic showers

In Figures 3, 4, 5 and 6 we present the total punchthrough probability of hadronic showers as a function of meters of iron equivalent for negative and positive pions, positive kaons and protons. The results with M1 at full field (3 T) and M1 off (0 T) are compared. The numerical values of these measurements and additional measurements taken with M1 at half field (1.5 T) are presented in Appendix A.

These data are characterized by two distinct regions. For example, consider the 100 GeV/c π^- data (Fig. 4). For depths less than about 3 m iron eq., the curve has a steep slope which represents the absorption of the hadronic component of the shower as a function of increasing absorber depth. For depths greater than 3 m iron eq. the curve flattens out; this represents the presence of penetrating punchthrough muons produced as a component of the hadronic shower.

In these figures one observes a reduction in the total punchthrough probability with the M1 field at 3 T relative to that with M1 at 0 T. This effect can be explained, in part, by low energy shower particles curling in the magnetic field inside TRACAL and, in part, by punchthrough particles being deflected outside the detector acceptance by the fields of M1 and M2. For depths less than 10λ (< 1.69 m iron eq.), the geometrical acceptance of the RD5 detector is determined by the size of TRACAL, for depths greater than 10λ, it is determined by the height of the magnet M2. The limited acceptance is more pronounced when the M1 field is at 3 T; particles may exit the calorimeter at large angles and be deflected outside the acceptance of the magnet M2.

In order to estimate the effect of the finite detector acceptance on the measurement of the total

punchthrough probability, an additional GEANT simulation was run in which the size of TRACAL and the magnet M2 were expanded to cover the entire area (3.2×3.8 m^2) of the muon drift chambers. The reduction in the punchthrough probability caused by particles lost outside the detector acceptance was estimated by comparing the total punchthrough probability at a given depth obtained from the simulation with the enlarged geometry, to that obtained from the simulation with the normal RD5 geometry. It was found that, independent of incident hadron momentum, for the simulated events with M1 off, the reduction in the punchthrough probability inside TRACAL ($<$ 1.69 m Fe eq.) was less than a few percent and increased to $4.4 \pm 0.6\%$ at the muon station 1 and $5.7 \pm 2.3\%$ at the muon station 2. For simulated events with M1 at 3 T the reduction in the punchthrough probability at the muon station 1 was $7.3 \pm 1.4\%$ and increased to $51 \pm 6\%$ at the muon station 2.

We can conclude that the reduction in the punchthrough probability (see Figures 3, 4, 5 and 6) caused by magnetic field, observed for absorber depths greater than 10 λ (muon stations 1, 2 and 3), can be wholly explained by punchthrough particles being deflected outside the detector acceptance. The reduction in the punchthrough probability for absorber depths less than 10 λ (within TRACAL) can be almost entirely explained by low energy shower particles curling back inside TRACAL. As expected, the reduction in punchthrough due to magnetic field is largest for lower momentum data. For the 10 GeV/c π^- data, the reduction in the punchthrough probability at 1.43 m iron eq. was almost a factor 3.

The total punchthrough probability of 10 GeV/c negative pions, for both field conditions (3 T and 0 T), and 20 and 30 GeV/c negative pions, for a M1 field of 3 T, were only measured up to the level of Station 1 (approximately 10λ). This is because the background muons coming from pion decays upstream of the detector were not completely removed by our muon subtraction algorithm. We regard as muons those events having one minimum ionizing track in TRACAL and a penetration depth up to Station 3 (see Ref. [3] for details). For a large number of muons in the lower momentum pion beams, this definition fails because many of these muons are bent by the M2 magnetic field outside the acceptance of Station 3. The fraction of background muons lost from the 10 GeV/c pion beam was estimated by analyzing the 10 GeV/c muon data. It was found that 30% of these muons were bent out of the acceptance of the detector between Station 2 and Station 3 while another 5% were lost between Station 1 and Station 2.

Next, we compare the total punchthrough probability of positive pions and kaons. In Fig. 7, one sees that the punchthrough probability of 100 GeV/c positive pions is less than that of positive kaons, for a given depth. This difference can be explained by the fact that kaon-induced showers will contain more secondary kaons which have a higher probability to decay into muons [18]. Furthermore, the π^+ and K^+ inelastic cross sections per nucleon, at 100 GeV/c, are about 23 mb and 17 mb, respectively [17]. On average, positive pions will have a primary hard interaction earlier in TRACAL, relative to positive kaons, and, as a result, have a larger amount absorber available after the primary interaction to stop the remaining shower.

In Figures 8, 9 and 10 we compare the total punchthrough probability of simulated negative pions with the real data. The solid line indicates the simulation results with M1 at full field and the dotted line with M1 off. The statistical errors for the simulated data are shown at the last bin. The errors on all preceding bins are smaller. Figures 8 and 9 show the results obtained with hadronic shower generators GHEISHA and FLUKA, respectively. In Fig. 10 we present the results obtained with both GHEISHA and FLUKA compared with 10 GeV/c negative pion data. The scale of Fig. 10 only extends to 2 m of iron equivalent in order to magnify the area of interest for 10 GeV/c data. The agreement between both hadronic shower generators and the real data is good, with FLUKA exhibiting a somewhat better agreement at low momentum, i.e. 10 and 30 GeV/c.

The total punchthrough probability of 50 GeV/c positive kaons is compared, in Fig. 11, with results obtained using GHEISHA. The real data were taken with M1 at full field.

Finally, we investigate the muon composition of the punchthrough showers as a function of absorber depth. In Fig. 12, the muon component of simulated showers originating from 50 GeV/c negative pions is indicated by the dashed line. The particle identification information was recorded while running the simulation. The dashed line indicates the proportion of simulated events with a muon present either at that depth or a greater depth. Both hadronic shower generators predict that hadronic punchthrough dominates until about 10λ (1.69 m Fe eq.), and punchthrough muons at greater depths.

5.2 Shower Lateral Distributions

Further properties of hadronic showers were investigated, including the shower lateral distribution, as measured by TRACAL wires. Figure 13 shows the distribution of hit wires in TRACAL layers 8 and 21, at about 2.5λ and 7.5 λ, respectively. These layers were chosen to be representative of the shower at two different points: at the beginning and end of the shower development. The simulation results obtained with GHEISHA and FLUKA are compared with data. The incident beam particles were 50 GeV/c negative pions and the magnet M1 was off. Each TRACAL layer consisted of 48 anode wires strung in the center of drift cells; the wire pitch is 12.7 mm. As seen in Fig. 13 a), only the 32 central wires of layer 8 were instrumented. Figure 14 shows the same distribution just described but with the M1 field at 3 T. On each figure, 0 cm indicates the nominal beam position. The wire hit distributions in Figures 13 and 14 have all been normalized by the total number of events in order to better compare their shapes. It is seen that the simulation results agree well with the data.

5.3 Shower Multiplicity Distribution

In this section the total charged particle multiplicity as measured by TRACAL wires and RPC strips is compared with the results of simulation. Figure 15 shows the TRACAL hit wire multiplicity in layers 8 and 21 for 50 GeV/c negative pions compared with predictions of the simulation. The histograms are normalized by the total number of events. Figure 16 shows the same distributions for M1 at 3 T. The number of events with zero multiplicity are not shown. As before, these layers were chosen to be representative of the shower at the beginning and at the end of the shower development.

The multiplicity of hit RPC strips is presented in Fig. 17 for 30, 50, 100 and 300 GeV/c negative pions as the incident particles. The RPC chambers used were in the muon station 1, at a depth of 10λ. Again, the number of events with zero multiplicity are not shown. The experimental results are compared with the GEANT simulation. Both hadronic shower generators, GHEISHA and FLUKA, were used. The agreement of both hadronic shower generators are good. The apparent disagreement in Fig. 17 d), for RPC strip multiplicity greater than 30, is due to lack of statistics for the simulated data.

Next, we demand the presence of a muon by requiring that each punchthrough event also reaches Station 2. The results are presented in Fig. 18, for 30, 50, 100 and 300 GeV/c negative pions as the incident particles. Note that for 30 GeV/c incident pions, the punchthrough muon is accompanied by few additional hits in Station 1. In contrast, for the 300 GeV/c pion data, the muons reaching Station 2 are accompanied in Station 1 by a large number of additional hits, possibly soft hadrons and electrons, the remnant of the hadronic cascade.

6 Conclusions

We have measured the total punchthrough probability of hadronic showers produced by positive and negative pions, positive kaons and protons with primary momenta from 10 to 300 GeV/c. Measurements were made up to a depth of about 31λ, farther than measured by previous experiments. The dominant error in these measurements is the uncertainty in the subtraction of the muon contamination in the pion beam. The punchthrough probability at the muon station 2 (3.49 m iron eq.) and station 3 (5.29 m iron eq.) are most sensitive to this background. An appropriate systematic error has been added reflecting the uncertainty in the background subtraction.

The influence of a 3 T and 1.5 T magnetic field on hadronic punchthrough was experimentally investigated for the first time. The observed reduction in the punchthrough probability for absorber depths less than 10λ is predominately caused by low energy shower particles curling back inside TRACAL. On the other hand, the reduction in the punchthrough probability for absorber depths greater than 10λ can be explained by particles being deflected outside the RD5 detector acceptance.

The measurements have been compared with the results of a simulation of the RD5 detector using GEANT 3.21 and two different hadronic shower generators: GHEISHA and FLUKA. The GEANT energy thresholds used were: 1 MeV for all types of particles in the absorbers, and 10 keV for electrons and gammas in the sensitive volumes of the detectors. The measured quantities, including the total punchthrough probability, the lateral shower distribution and shower particle multiplicity, were compaired with the simulation. The general agreement between the simulation program and all aspects of the punchthrough study in RD5, gives one confidence that this GEANT-based simulation program can be used to make predictions for the design of LHC detectors.

Acknowledgments

We would like to thank W. Ko and the High Energy Physics Group of the University of California Davis for the use of their computers in performing the GEANT3.21 simulations. We would also like to thank R. Jenkins for his assistance in running the simulations. For their support in the construction of RD5 and during the actual runs we thank S. Lazic, D. Peach, P. Pétiot, J. Pothier, B. Powell, A. Tusi and G. Waurick.

The authors also acknowledge the support of the following funding agencies:

- Deutsches Bundesministerium für Forschung und Technologie,
- Hungarian Academy of Science under grant OTKA-4389,
- Istituto Nazionale di Fisica Nucleare, Italy,
- Polish Committee for Scientific Research under grants KBN-PB-2 0422 91 01 and KBN-SPUB-206/93.
- Spanish CICYT under grants AEN92-0829-E and AEN-93-0954-E,
- US Department of Energy – contract numbers DE-AC02-76CH00016, DE-FG05-91ER40617 and DE-FG02-92ER40697,
- Texas National Research Laboratory Commission – award numbers RGFY92-118 and RGFY93-312A,

References

[1] A. Nisati, *Muon Rates at the LHC*, Proc. LHC Workshop Aachen, 1990, eds. G. Jarlskog and D. Rein, **CERN 90-10**.

[2] M. Della Negra et al., *Study of Muon Triggers and Momentum Reconstruction in a Strong Magnetic Field for a Muon Detector at LHC*, **CERN/DRDC/90-36, DRDC/P7**.

[3] M. Aalste et al., Z.Phys. **C60** (1993) 1.

[4] C. Albajar et al., *Measurement of Momentum and Angular Distribution of Punchthrough Muons at the RD5 Experiment*, in preparation.

[5] C. Albajar et al., *Electromagnetic Secondaries in the Detection of High Energy Muons*, **CERN-PPE/94-204** (1994).

[6] The RD5 Collaboration, *Status Report of the RD5 Experiment*, **CERN/DRDC/93-49**.

[7] The CMS Collaboration, *The Compact Muon Solenoid Technical Proposal*, **CERN/LHCC 94-38**.

[8] R. Santonico, R. Cardarelli, Nucl. Instr. and Meth. **A187** (1981)377;
R. Cardarelli et al., Nucl. Instr. and Meth. **A263** (1988) 20.

[9] H. Van der Graaf, Nucl. Instr. and Meth. **A307** (1991) 220;
F. Bakker et al., Nucl. Instr. and Meth. **A330** (1993) 44.

[10] K. Eggert et al., Nucl. Instr. and Meth. **176** (1980) 217;
C. Albajar et al., Z.Phys. **C44** (1989) 15.

[11] G.L. Bencze et al., Nucl. Instr. and Meth. **A340** (1994) 466.

[12] M. Aguilar-Benitez et al., Nucl. Instr. and Meth. **A258** (1997) 26.

[13] T. Moers et al., Nucl. Instr. and Meth. **A345** (1994) 474.

[14] R. Brun, M. Hansroul and L.C. Lassalle, GEANT User's Guide,**CERN DD/EE/82**, (1982);
CERN Program Library Long Writeup W5013.

[15] H. Fesefeldt, *The Simulation of Hadronic Showers - Physics and Applications*, RWTH Aachen Report **PITHA 85/02** (1985);
H. Fesefeldt, Proc. 3rd Pisa Meeting on Advanced Detectors, Castiglione della Pescaia, 1986;
Nucl. Instr. and Meth. **A263** (1988) 114.

[16] A. Fassò, A. Ferrari, J. Ranft, P.R. Sala, G.R. Stevenson and J.M. Zavula. FLUKA92. In *Proceedings of the Workshop on Simulating Accelerator Radiation Environments*, Santa Fe, USA, 11-15 January 1993.

[17] Phys. Rev. D, Vol. 45 Part II, Review of Particle Properties, (1992) p. III.86 - III.88.

[18] P.H. Sandler et al., Phys. Rev. **D42** (1990) 759.

A Total Punchthrough Probability Numerical Results Tabulated

The tables below contain the results of measurements of the total punchthrough probability of hadronic showers as a function of absorber depth. These are the results after all know muon backgrounds have been subtracted. The error is the sum of the statistical error and an additional error reflecting an uncertainty in subtracting the muon background. The results below have not been corrected for the detector acceptance.

Table 3: Total punchthrough probability of 10, 20, 30 and 50 GeV/c negative pions, magnet M1 off.

Iron eq. (m)	10 GeV/c	20 GeV/c	30 GeV/c	50 GeV/c
0.15	0.99978 $\pm$0.00006	0.9967 $\pm$0.0002	0.9984 $\pm$0.0001	0.99993 $\pm$0.00003
0.19	0.9921 $\pm$0.0004	0.9922 $\pm$0.0003	0.9952 $\pm$0.0002	0.99985 $\pm$0.00005
0.23	0.9769 $\pm$0.0006	0.9851 $\pm$0.0004	0.9919 $\pm$0.0003	0.9992 $\pm$0.0001
0.27	0.9537 $\pm$0.0009	0.9745 $\pm$0.0006	0.9871 $\pm$0.0003	0.9983 $\pm$0.0002
0.31	0.926 $\pm$0.001	0.9619 $\pm$0.0008	0.9812 $\pm$0.0004	0.9971 $\pm$0.0002
0.35	0.890 $\pm$0.001	0.9483 $\pm$0.0009	0.9747 $\pm$0.0005	0.9943 $\pm$0.0003
0.39	0.843 $\pm$0.002	0.929 $\pm$0.001	0.9656 $\pm$0.0006	0.9908 $\pm$0.0004
0.43	0.783 $\pm$0.002	0.900 $\pm$0.001	0.9503 $\pm$0.0007	0.9856 $\pm$0.0004
0.47	0.733 $\pm$0.002	0.870 $\pm$0.001	0.9324 $\pm$0.0008	0.9788 $\pm$0.0005
0.51	0.669 $\pm$0.003	0.829 $\pm$0.002	0.9071 $\pm$0.0009	0.9686 $\pm$0.0006
0.55	0.600 $\pm$0.003	0.784 $\pm$0.002	0.878 $\pm$0.001	0.9567 $\pm$0.0007
0.59	0.532 $\pm$0.003	0.728 $\pm$0.002	0.836 $\pm$0.001	0.9366 $\pm$0.0009
0.63	0.470 $\pm$0.004	0.670 $\pm$0.002	0.787 $\pm$0.001	0.906 $\pm$0.001
0.71	0.395 $\pm$0.004	0.596 $\pm$0.002	0.723 $\pm$0.001	0.864 $\pm$0.001
0.79	0.333 $\pm$0.004	0.526 $\pm$0.002	0.656 $\pm$0.002	0.812 $\pm$0.001
0.87	0.270 $\pm$0.005	0.443 $\pm$0.002	0.568 $\pm$0.002	0.730 $\pm$0.002
0.95	0.201 $\pm$0.005	0.350 $\pm$0.002	0.466 $\pm$0.002	0.631 $\pm$0.002
1.03	0.126 $\pm$0.005	0.246 $\pm$0.002	0.351 $\pm$0.002	0.515 $\pm$0.002
1.11	0.090 $\pm$0.006	0.188 $\pm$0.002	0.278 $\pm$0.001	0.428 $\pm$0.002
1.19	0.071 $\pm$0.006	0.153 $\pm$0.001	0.232 $\pm$0.001	0.367 $\pm$0.002
1.27	0.051 $\pm$0.006	0.114 $\pm$0.001	0.178 $\pm$0.001	0.295 $\pm$0.002
1.35	0.036 $\pm$0.006	0.081 $\pm$0.001	0.133 $\pm$0.001	0.230 $\pm$0.002
1.43	0.029 $\pm$0.006	0.064 $\pm$0.001	0.1061 $\pm$0.0010	0.187 $\pm$0.001
1.51	0.021 $\pm$0.006	0.0459 $\pm$0.0009	0.0790 $\pm$0.0009	0.144 $\pm$0.001
1.59	0.013 $\pm$0.006	0.0260 $\pm$0.0007	0.0470 $\pm$0.0007	0.092 $\pm$0.001
1.69		0.0153 $\pm$0.0002	0.0291 $\pm$0.0002	0.0673 $\pm$0.0003
2.29		0.00296 $\pm$0.00008	0.00602 $\pm$0.00010	0.0141 $\pm$0.0002
2.89		0.00096 $\pm$0.00005	0.00177 $\pm$0.00006	0.0039 $\pm$0.0001
3.49		0.00050 $\pm$0.00004	0.00086 $\pm$0.00005	0.00171 $\pm$0.00008
5.29		0.00013 $\pm$0.00003	0.00036 $\pm$0.00005	0.00061 $\pm$0.00007

Table 4: Total punchthrough probability of 10, 20, 30 and 50 GeV/c negative pions, M1 field 3 T.

Iron eq. (m)	10 GeV/c	20 GeV/c	30 GeV/c	50 GeV/c
0.15	0.9993 ±0.0001	0.99981 ±0.00005	0.9965 ±0.0002	0.99997 ±0.00002
0.19	0.9944 ±0.0003	0.9942 ±0.0003	0.9937 ±0.0003	0.9990 ±0.0001
0.23	0.9803 ±0.0006	0.9846 ±0.0004	0.9898 ±0.0004	0.9978 ±0.0002
0.27	0.9584 ±0.0009	0.9695 ±0.0006	0.9842 ±0.0004	0.9962 ±0.0002
0.31	0.932 ±0.001	0.9523 ±0.0008	0.9774 ±0.0005	0.9944 ±0.0003
0.35	0.892 ±0.001	0.9347 ±0.0009	0.9690 ±0.0006	0.9921 ±0.0003
0.39	0.838 ±0.002	0.909 ±0.001	0.9571 ±0.0007	0.9886 ±0.0004
0.43	0.774 ±0.002	0.874 ±0.001	0.9383 ±0.0008	0.9830 ±0.0005
0.47	0.718 ±0.002	0.839 ±0.001	0.9165 ±0.0010	0.9746 ±0.0006
0.51	0.649 ±0.002	0.792 ±0.001	0.887 ±0.001	0.9619 ±0.0007
0.55	0.573 ±0.002	0.739 ±0.002	0.852 ±0.001	0.9468 ±0.0008
0.59	0.500 ±0.002	0.679 ±0.002	0.807 ±0.001	0.9234 ±0.0010
0.63	0.437 ±0.002	0.618 ±0.002	0.754 ±0.002	0.893 ±0.001
0.71	0.361 ±0.002	0.540 ±0.002	0.685 ±0.002	0.854 ±0.001
0.79	0.298 ±0.002	0.469 ±0.002	0.615 ±0.002	0.812 ±0.001
0.87	0.236 ±0.002	0.388 ±0.002	0.526 ±0.002	0.719 ±0.002
0.95	0.169 ±0.002	0.298 ±0.002	0.425 ±0.002	0.609 ±0.002
1.03	0.098 ±0.002	0.197 ±0.002	0.311 ±0.002	0.482 ±0.002
1.11	0.065 ±0.002	0.143 ±0.002	0.244 ±0.002	0.394 ±0.002
1.19	0.047 ±0.002	0.110 ±0.002	0.202 ±0.001	0.330 ±0.002
1.27	0.027 ±0.002	0.071 ±0.002	0.154 ±0.001	0.253 ±0.002
1.35	0.016 ±0.002	0.049 ±0.002	0.113 ±0.001	0.201 ±0.001
1.43	0.010 ±0.002	0.036 ±0.002	0.088 ±0.001	0.163 ±0.001
1.51		0.022 ±0.002	0.0644 ±0.0009	0.124 ±0.001
1.59			0.0357 ±0.0007	0.0767 ±0.0010
1.69			0.0197 ±0.0005	0.0527 ±0.0003
2.29			0.0027 ±0.0003	0.0105 ±0.0002
2.89				0.0021 ±0.0001
3.49				0.00076 ±0.00009
5.29				0.00020 ±0.00008

Table 5: Total punchthrough probability of 100, 200 and 300 GeV/c negative pions, magnet M1 off.

Iron eq. (m)	100 GeV/c	200 GeV/c	300 GeV/c
0.15	0.99956 ±0.00007	1.000000±0.000001	0.99997 ±0.00003
0.19	0.99931 ±0.00008	0.99997 ±0.00003	0.99997 ±0.00003
0.23	0.99903 ±0.00010	0.99987 ±0.00006	0.99995 ±0.00004
0.27	0.9981 ±0.0001	0.99979 ±0.00008	0.99987 ±0.00006
0.31	0.9968 ±0.0002	0.9995 ±0.0001	0.99970 ±0.00009
0.35	0.9955 ±0.0002	0.9993 ±0.0001	0.9995 ±0.0001
0.39	0.9936 ±0.0002	0.9991 ±0.0002	0.9993 ±0.0001
0.43	0.9903 ±0.0003	0.9987 ±0.0002	0.9990 ±0.0002
0.47	0.9871 ±0.0003	0.9982 ±0.0002	0.9988 ±0.0002
0.51	0.9836 ±0.0004	0.9975 ±0.0003	0.9984 ±0.0002
0.55	0.9800 ±0.0004	0.9968 ±0.0003	0.9980 ±0.0002
0.59	0.9723 ±0.0005	0.9947 ±0.0004	0.9975 ±0.0003
0.63	0.9646 ±0.0006	0.9926 ±0.0005	0.9967 ±0.0003
0.71	0.9323 ±0.0008	0.9904 ±0.0005	0.9954 ±0.0004
0.79	0.9001 ±0.0009	0.9807 ±0.0007	0.9929 ±0.0005
0.87	0.855 ±0.001	0.964 ±0.001	0.9854 ±0.0007
0.95	0.809 ±0.001	0.947 ±0.001	0.9744 ±0.0009
1.03	0.744 ±0.001	0.920 ±0.001	0.959 ±0.001
1.11	0.657 ±0.001	0.894 ±0.002	0.931 ±0.001
1.19	0.571 ±0.002	0.839 ±0.002	0.895 ±0.002
1.27	0.486 ±0.002	0.769 ±0.002	0.845 ±0.002
1.35	0.403 ±0.002	0.678 ±0.003	0.776 ±0.002
1.43	0.332 ±0.001	0.593 ±0.003	0.694 ±0.003
1.51	0.262 ±0.001	0.509 ±0.003	0.611 ±0.003
1.59	0.182 ±0.001	0.387 ±0.003	0.499 ±0.003
1.69	0.1215 ±0.0005	0.291 ±0.002	0.430 ±0.002
2.29	0.0282 ±0.0003	0.075 ±0.001	0.123 ±0.001
2.89	0.0086 ±0.0001	0.0194 ±0.0007	0.0324 ±0.0008
3.49	0.0041 ±0.0001	0.0071 ±0.0006	0.0126 ±0.0007
5.29	0.00227 ±0.00009	0.0030 ±0.0006	0.0055 ±0.0006

Table 6: Total punchthrough probability of 100, 200 and 300 GeV/c negative pions, M1 field 3 T.

Iron eq. (m)	100 GeV/c	200 GeV/c	300 GeV/c
0.15	0.99975 ±0.00007	0.99984 ±0.00006	1.000000±0.000001
0.19	0.9995 ±0.0001	0.99972 ±0.00008	1.000000±0.000001
0.23	0.9990 ±0.0001	0.9995 ±0.0001	0.99998 ±0.00003
0.27	0.9982 ±0.0002	0.9991 ±0.0001	0.99991 ±0.00005
0.31	0.9974 ±0.0002	0.9987 ±0.0002	0.99979 ±0.00007
0.35	0.9966 ±0.0002	0.9983 ±0.0002	0.99968 ±0.00009
0.39	0.9953 ±0.0003	0.9978 ±0.0002	0.9995 ±0.0001
0.43	0.9939 ±0.0003	0.9970 ±0.0002	0.9994 ±0.0001
0.47	0.9918 ±0.0004	0.9964 ±0.0003	0.9992 ±0.0001
0.51	0.9885 ±0.0005	0.9954 ±0.0003	0.9988 ±0.0002
0.55	0.9852 ±0.0005	0.9945 ±0.0003	0.9984 ±0.0002
0.59	0.9762 ±0.0007	0.9921 ±0.0004	0.9981 ±0.0002
0.63	0.9655 ±0.0008	0.9893 ±0.0005	0.9970 ±0.0003
0.71	0.9465 ±0.0010	0.9843 ±0.0006	0.9955 ±0.0003
0.79	0.898 ±0.001	0.9711 ±0.0008	0.9929 ±0.0004
0.87	0.850 ±0.002	0.9534 ±0.0010	0.9845 ±0.0006
0.95	0.781 ±0.002	0.926 ±0.001	0.9718 ±0.0008
1.03	0.709 ±0.002	0.889 ±0.001	0.953 ±0.001
1.11	0.660 ±0.002	0.856 ±0.002	0.925 ±0.001
1.19	0.580 ±0.002	0.794 ±0.002	0.886 ±0.002
1.27	0.485 ±0.002	0.717 ±0.002	0.830 ±0.002
1.35	0.389 ±0.002	0.622 ±0.002	0.768 ±0.002
1.43	0.324 ±0.002	0.538 ±0.002	0.689 ±0.002
1.51	0.257 ±0.002	0.452 ±0.002	0.610 ±0.002
1.59	0.164 ±0.002	0.323 ±0.002	0.491 ±0.003
1.69	0.1035 ±0.0006	0.227 ±0.001	0.377 ±0.002
2.29	0.0236 ±0.0003	0.0576 ±0.0008	0.108 ±0.002
2.89	0.0057 ±0.0002	0.0140 ±0.0006	0.0257 ±0.0008
3.49	0.0023 ±0.0001	0.0054 ±0.0006	0.0081 ±0.0005
5.29	0.0008 ±0.0001	0.0023 ±0.0006	0.0027 ±0.0004

Table 7: Total punchthrough probability of 30, 100 and 300 GeV/c positive pions, magnet M1 off.

Iron eq. (m)	30 GeV/c	100 GeV/c	300 GeV/c
0.15	0.99933 ±0.00009	0.99999 ±0.00002	0.999999±0.000003
0.19	0.9976 ±0.0002	0.99947 ±0.00009	0.999999±0.000004
0.23	0.9950 ±0.0002	0.9981 ±0.0002	0.99997 ±0.00002
0.27	0.9911 ±0.0003	0.9964 ±0.0002	0.99994 ±0.00004
0.31	0.9861 ±0.0004	0.9949 ±0.0003	0.99983 ±0.00006
0.35	0.9800 ±0.0005	0.9939 ±0.0003	0.99965 ±0.00008
0.39	0.9707 ±0.0006	0.9928 ±0.0003	0.9994 ±0.0001
0.43	0.9558 ±0.0007	0.9917 ±0.0004	0.9992 ±0.0001
0.47	0.9383 ±0.0008	0.9905 ±0.0004	0.9991 ±0.0001
0.51	0.9131 ±0.0010	0.9886 ±0.0004	0.9988 ±0.0001
0.55	0.884 ±0.001	0.9864 ±0.0004	0.9985 ±0.0002
0.59	0.843 ±0.001	0.9825 ±0.0005	0.9981 ±0.0002
0.63	0.794 ±0.001	0.9743 ±0.0006	0.9972 ±0.0002
0.71	0.730 ±0.002	0.9617 ±0.0007	0.9959 ±0.0003
0.79	0.662 ±0.002	0.9403 ±0.0009	0.9934 ±0.0003
0.87	0.574 ±0.002	0.895 ±0.001	0.9861 ±0.0005
0.95	0.471 ±0.002	0.833 ±0.001	0.9748 ±0.0007
1.03	0.355 ±0.002	0.754 ±0.002	0.9581 ±0.0009
1.11	0.280 ±0.002	0.674 ±0.002	0.932 ±0.001
1.19	0.234 ±0.001	0.606 ±0.002	0.897 ±0.001
1.27	0.180 ±0.001	0.519 ±0.002	0.848 ±0.002
1.35	0.135 ±0.001	0.429 ±0.002	0.779 ±0.002
1.43	0.108 ±0.001	0.358 ±0.002	0.698 ±0.002
1.51	0.0807 ±0.0009	0.287 ±0.002	0.618 ±0.002
1.59	0.0490 ±0.0007	0.198 ±0.002	0.505 ±0.002
1.69	0.0307 ±0.0002	0.1373 ±0.0007	0.427 ±0.001
2.29	0.00642 ±0.00008	0.0298 ±0.0004	0.120 ±0.001
2.89	0.00176 ±0.00006	0.0076 ±0.0002	0.0323 ±0.0007
3.49	0.00081 ±0.00005	0.0033 ±0.0001	0.0123 ±0.0006
5.29	0.00037 ±0.00004	0.0016 ±0.0001	0.0052 ±0.0005

Table 8: Total punchthrough probability of 30, 100 and 300 GeV/c positive pions, M1 field 3 T.

Iron eq. (m)	30 GeV/c	100 GeV/c	300 GeV/c
0.15	0.9987 $\pm$0.0001	0.99984 $\pm$0.00007	1.000000$\pm$0.000001
0.19	0.9971 $\pm$0.0002	0.9994 $\pm$0.0001	1.000000$\pm$0.000002
0.23	0.9942 $\pm$0.0003	0.9987 $\pm$0.0002	0.99999 $\pm$0.00002
0.27	0.9895 $\pm$0.0004	0.9977 $\pm$0.0003	0.99994 $\pm$0.00004
0.31	0.9834 $\pm$0.0004	0.9969 $\pm$0.0003	0.99976 $\pm$0.00008
0.35	0.9763 $\pm$0.0005	0.9960 $\pm$0.0003	0.99965 $\pm$0.00009
0.39	0.9652 $\pm$0.0006	0.9947 $\pm$0.0004	0.9995 $\pm$0.0001
0.43	0.9485 $\pm$0.0008	0.9935 $\pm$0.0004	0.9992 $\pm$0.0001
0.47	0.9277 $\pm$0.0009	0.9918 $\pm$0.0005	0.9989 $\pm$0.0002
0.51	0.899 $\pm$0.001	0.9893 $\pm$0.0006	0.9987 $\pm$0.0002
0.55	0.865 $\pm$0.001	0.9864 $\pm$0.0006	0.9983 $\pm$0.0002
0.59	0.822 $\pm$0.001	0.9806 $\pm$0.0007	0.9978 $\pm$0.0002
0.63	0.771 $\pm$0.001	0.9697 $\pm$0.0009	0.9969 $\pm$0.0003
0.71	0.703 $\pm$0.002	0.954 $\pm$0.001	0.9956 $\pm$0.0003
0.79	0.634 $\pm$0.002	0.927 $\pm$0.001	0.9931 $\pm$0.0004
0.87	0.546 $\pm$0.002	0.871 $\pm$0.002	0.9855 $\pm$0.0006
0.95	0.443 $\pm$0.002	0.801 $\pm$0.002	0.9736 $\pm$0.0008
1.03	0.328 $\pm$0.002	0.716 $\pm$0.002	0.956 $\pm$0.001
1.11	0.257 $\pm$0.002	0.635 $\pm$0.003	0.929 $\pm$0.001
1.19	0.209 $\pm$0.001	0.567 $\pm$0.003	0.894 $\pm$0.002
1.27	0.154 $\pm$0.001	0.483 $\pm$0.003	0.844 $\pm$0.002
1.35	0.118 $\pm$0.001	0.398 $\pm$0.003	0.775 $\pm$0.002
1.43	0.094 $\pm$0.001	0.330 $\pm$0.003	0.692 $\pm$0.002
1.51	0.0695 $\pm$0.0009	0.261 $\pm$0.002	0.608 $\pm$0.002
1.59	0.0399 $\pm$0.0007	0.173 $\pm$0.002	0.487 $\pm$0.002
1.69	0.0275 $\pm$0.0002	0.1099 $\pm$0.0009	0.391 $\pm$0.002
2.29	0.00498 $\pm$0.00009	0.0232 $\pm$0.0005	0.112 $\pm$0.001
2.89	0.00104 $\pm$0.00006	0.0051 $\pm$0.0003	0.0262 $\pm$0.0007
3.49	0.00048 $\pm$0.00006	0.0017 $\pm$0.0003	0.0084 $\pm$0.0005
5.29	0.00013 $\pm$0.00005	0.0005 $\pm$0.0002	0.0028 $\pm$0.0005

Table 9: Total punchthrough probability of 100 GeV/c positive kaons and 100 and 300 GeV/c protons, magnet M1 off.

Iron eq. (m)	100 GeV/c K^+	100 GeV/c proton	300 GeV/c proton
0.15	0.99994 ±0.00004	0.999999±0.000005	1.000000±0.000002
0.19	0.99974 ±0.00008	0.999999±0.000005	1.000000±0.000002
0.23	0.9994 ±0.0001	0.999999±0.000005	0.99999 ±0.00002
0.27	0.9989 ±0.0002	0.999999±0.000005	0.99997 ±0.00003
0.31	0.9984 ±0.0002	0.99999 ±0.00001	0.99997 ±0.00003
0.35	0.9980 ±0.0002	0.99997 ±0.00002	0.99997 ±0.00003
0.39	0.9976 ±0.0002	0.99995 ±0.00003	0.99997 ±0.00003
0.43	0.9970 ±0.0003	0.99987 ±0.00004	0.99997 ±0.00003
0.47	0.9964 ±0.0003	0.99956 ±0.00008	0.99995 ±0.00004
0.51	0.9952 ±0.0003	0.9990 ±0.0001	0.99993 ±0.00005
0.55	0.9940 ±0.0004	0.9982 ±0.0002	0.99990 ±0.00006
0.59	0.9886 ±0.0005	0.9960 ±0.0002	0.99988 ±0.00006
0.63	0.9833 ±0.0007	0.9901 ±0.0004	0.99980 ±0.00008
0.71	0.9779 ±0.0007	0.9805 ±0.0005	0.9996 ±0.0001
0.79	0.953 ±0.001	0.9614 ±0.0007	0.9986 ±0.0002
0.87	0.918 ±0.001	0.915 ±0.001	0.9936 ±0.0005
0.95	0.882 ±0.002	0.853 ±0.001	0.9855 ±0.0007
1.03	0.831 ±0.002	0.772 ±0.002	0.9731 ±0.0009
1.11	0.790 ±0.002	0.686 ±0.002	0.947 ±0.001
1.19	0.715 ±0.002	0.609 ±0.002	0.912 ±0.002
1.27	0.620 ±0.002	0.508 ±0.002	0.862 ±0.002
1.35	0.525 ±0.003	0.426 ±0.002	0.789 ±0.002
1.43	0.451 ±0.003	0.356 ±0.002	0.705 ±0.003
1.51	0.376 ±0.002	0.287 ±0.002	0.621 ±0.003
1.59	0.269 ±0.002	0.199 ±0.002	0.506 ±0.003
1.69	0.197 ±0.001	0.141 ±0.001	0.390 ±0.003
2.29	0.0521 ±0.0007	0.0298 ±0.0007	0.099 ±0.002
2.89	0.0150 ±0.0004	0.0073 ±0.0003	0.0274 ±0.0009
3.49	0.0068 ±0.0003	0.0030 ±0.0002	0.0119 ±0.0006
5.29	0.0040 ±0.0002	0.0013 ±0.0001	0.0061 ±0.0004

Table 10: Total punchthrough probability of 100 GeV/c positive kaons and 100 and 300 GeV/c protons, M1 field 3 T.

Iron eq. (m)	100 GeV/c K^+	100 GeV/c proton	300 GeV/c proton
0.15	0.99978 ±0.00007	1.000000±0.000001	0.99998 ±0.00002
0.19	0.99955 ±0.00009	1.000000±0.000001	0.99998 ±0.00002
0.23	0.9992 ±0.0001	1.000000±0.000002	0.99998 ±0.00002
0.27	0.9987 ±0.0002	0.99998 ±0.00002	0.99998 ±0.00002
0.31	0.9984 ±0.0002	0.99997 ±0.00003	0.99998 ±0.00002
0.35	0.9980 ±0.0002	0.99994 ±0.00004	0.99998 ±0.00002
0.39	0.9975 ±0.0002	0.99986 ±0.00006	0.99998 ±0.00002
0.43	0.9970 ±0.0002	0.9995 ±0.0001	0.99996 ±0.00003
0.47	0.9961 ±0.0003	0.9990 ±0.0001	0.99996 ±0.00003
0.51	0.9946 ±0.0003	0.9980 ±0.0002	0.99995 ±0.00003
0.55	0.9930 ±0.0004	0.9968 ±0.0003	0.99994 ±0.00004
0.59	0.9851 ±0.0005	0.9935 ±0.0004	0.99993 ±0.00004
0.63	0.9772 ±0.0007	0.9852 ±0.0006	0.99979 ±0.00007
0.71	0.9694 ±0.0008	0.9726 ±0.0008	0.9995 ±0.0001
0.79	0.937 ±0.001	0.947 ±0.001	0.9987 ±0.0002
0.87	0.894 ±0.001	0.892 ±0.001	0.9929 ±0.0004
0.95	0.851 ±0.002	0.822 ±0.002	0.9830 ±0.0006
1.03	0.795 ±0.002	0.734 ±0.002	0.9678 ±0.0009
1.11	0.753 ±0.002	0.647 ±0.002	0.940 ±0.001
1.19	0.675 ±0.002	0.574 ±0.002	0.901 ±0.001
1.27	0.581 ±0.002	0.483 ±0.002	0.846 ±0.002
1.35	0.488 ±0.002	0.392 ±0.002	0.769 ±0.002
1.43	0.415 ±0.002	0.321 ±0.002	0.678 ±0.002
1.51	0.341 ±0.002	0.250 ±0.002	0.587 ±0.002
1.59	0.232 ±0.002	0.160 ±0.002	0.456 ±0.002
1.69	0.1637 ±0.0008	0.105 ±0.001	0.340 ±0.002
2.29	0.0431 ±0.0005	0.0188 ±0.0006	0.085 ±0.001
2.89	0.0112 ±0.0003	0.0036 ±0.0003	0.0197 ±0.0007
3.49	0.0049 ±0.0002	0.0014 ±0.0002	0.0079 ±0.0004
5.29	0.0028 ±0.0001	0.0005 ±0.0001	0.0036 ±0.0003

Table 11: Total punchthrough probability of 30, 100 and 300 GeV/c negative pions and 100 GeV/c positive pions, M1 field 1.5 T

Iron eq. (m)	30 GeV/c π^-	100 GeV/c π^-	300 GeV/c π^-	100 GeV/c π^+
0.15	0.9969 ±0.0002	0.99992 ±0.00003	0.99998 ±0.00003	0.9990 ±0.0001
0.19	0.9939 ±0.0003	0.99977 ±0.00006	0.99997 ±0.00003	0.9965 ±0.0002
0.23	0.9901 ±0.0004	0.99946 ±0.00009	0.99987 ±0.00006	0.9926 ±0.0003
0.27	0.9846 ±0.0004	0.9989 ±0.0001	0.99965 ±0.00010	0.9880 ±0.0004
0.31	0.9779 ±0.0005	0.9983 ±0.0001	0.9994 ±0.0001	0.9852 ±0.0005
0.35	0.9705 ±0.0006	0.9976 ±0.0002	0.9992 ±0.0001	0.9838 ±0.0005
0.39	0.9595 ±0.0007	0.9967 ±0.0002	0.9989 ±0.0002	0.9820 ±0.0005
0.43	0.9423 ±0.0008	0.9955 ±0.0002	0.9987 ±0.0002	0.9803 ±0.0005
0.47	0.9224 ±0.0009	0.9940 ±0.0003	0.9984 ±0.0002	0.9786 ±0.0006
0.51	0.894 ±0.001	0.9914 ±0.0003	0.9979 ±0.0002	0.9760 ±0.0006
0.55	0.861 ±0.001	0.9887 ±0.0004	0.9974 ±0.0003	0.9733 ±0.0006
0.59	0.818 ±0.001	0.9813 ±0.0005	0.9965 ±0.0003	0.9662 ±0.0007
0.63	0.767 ±0.001	0.9723 ±0.0006	0.9954 ±0.0004	0.9576 ±0.0008
0.71	0.701 ±0.002	0.9564 ±0.0007	0.9937 ±0.0004	0.9422 ±0.0009
0.79	0.632 ±0.002	0.915 ±0.001	0.9892 ±0.0005	0.902 ±0.001
0.87	0.544 ±0.002	0.871 ±0.001	0.9828 ±0.0007	0.860 ±0.001
0.95	0.443 ±0.002	0.806 ±0.001	0.9715 ±0.0009	0.798 ±0.002
1.03	0.329 ±0.002	0.739 ±0.002	0.954 ±0.001	0.733 ±0.002
1.11	0.260 ±0.002	0.691 ±0.002	0.938 ±0.001	0.686 ±0.002
1.19	0.216 ±0.001	0.610 ±0.002	0.900 ±0.002	0.606 ±0.002
1.27	0.166 ±0.001	0.516 ±0.002	0.850 ±0.002	0.510 ±0.002
1.35	0.124 ±0.001	0.417 ±0.002	0.777 ±0.002	0.419 ±0.002
1.43	0.097 ±0.001	0.349 ±0.002	0.696 ±0.002	0.352 ±0.002
1.51	0.0719 ±0.0009	0.280 ±0.002	0.614 ±0.003	0.284 ±0.002
1.59	0.0423 ±0.0007	0.186 ±0.001	0.485 ±0.003	0.191 ±0.002
1.69	0.0236 ±0.0002	0.1224 ±0.0006	0.391 ±0.001	0.1206 ±0.0009
2.29	0.0047 ±0.0001	0.0283 ±0.0003	0.108 ±0.001	0.0276 ±0.0005
2.89	0.0016 ±0.0001	0.0077 ±0.0002	0.0278 ±0.0006	0.0076 ±0.0003
3.49	0.0009 ±0.0001	0.0036 ±0.0002	0.0104 ±0.0004	0.0038 ±0.0002
5.29	0.00043 ±0.00010	0.0015 ±0.0001	0.0040 ±0.0003	0.0020 ±0.0002

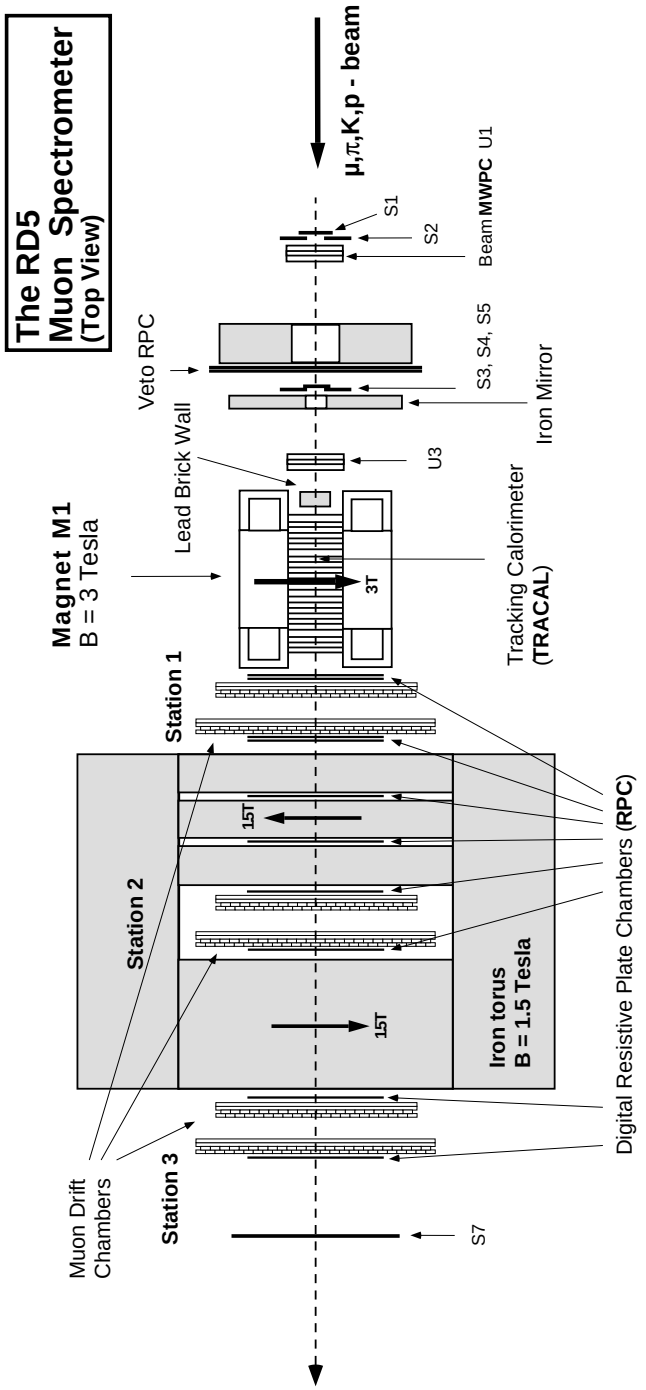

Figure 1: Schematic of the RD5 detector in its 1993 configuration.

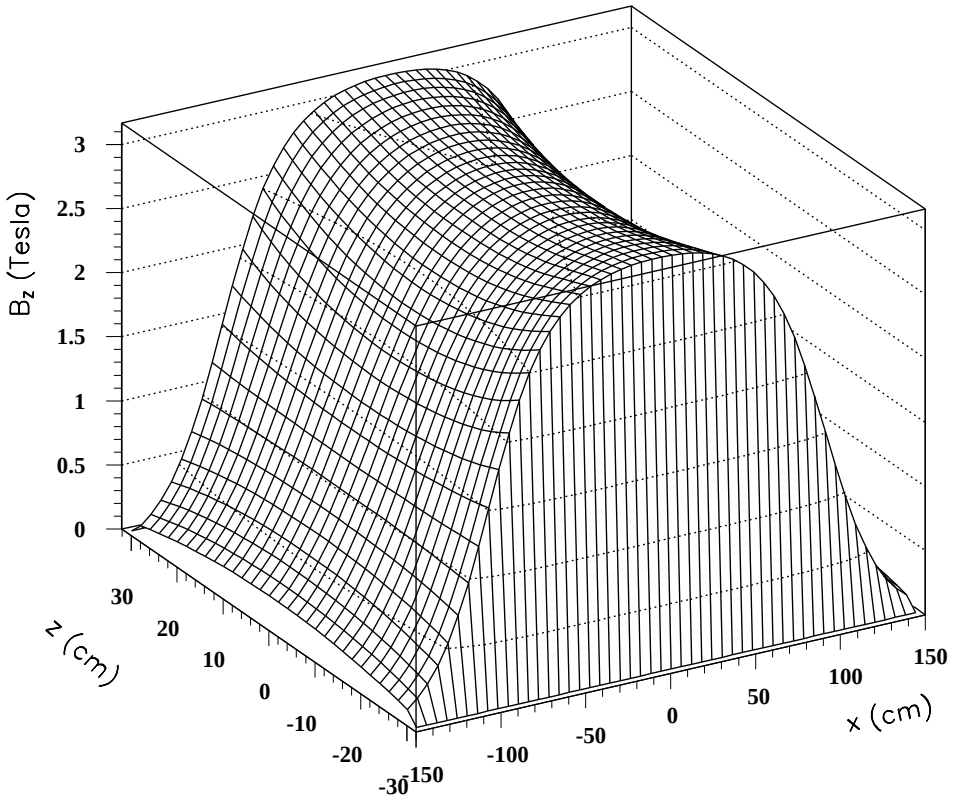

Figure 2: The z-component of the magnetic field in M1, plotted as a function of x and z. The x-direction is parallel to the beam, while z-direction is transverse to the beam.

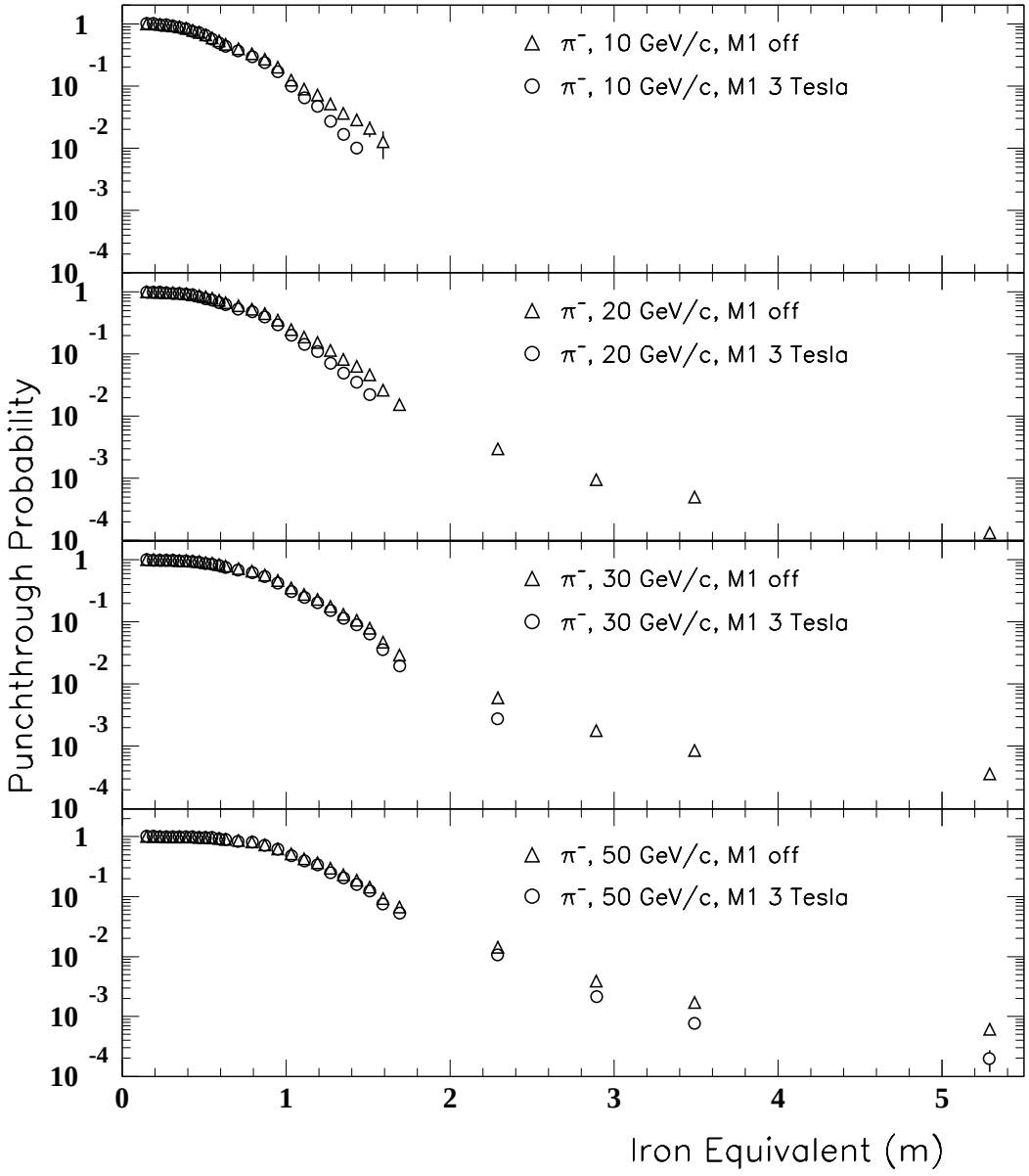

Figure 3: Total punchthrough probability as a function of meters of iron equivalent for 10, 20, 30 and 50 GeV/c negative pions. We compare data taken with the M1 field at 3 T and M1 off.

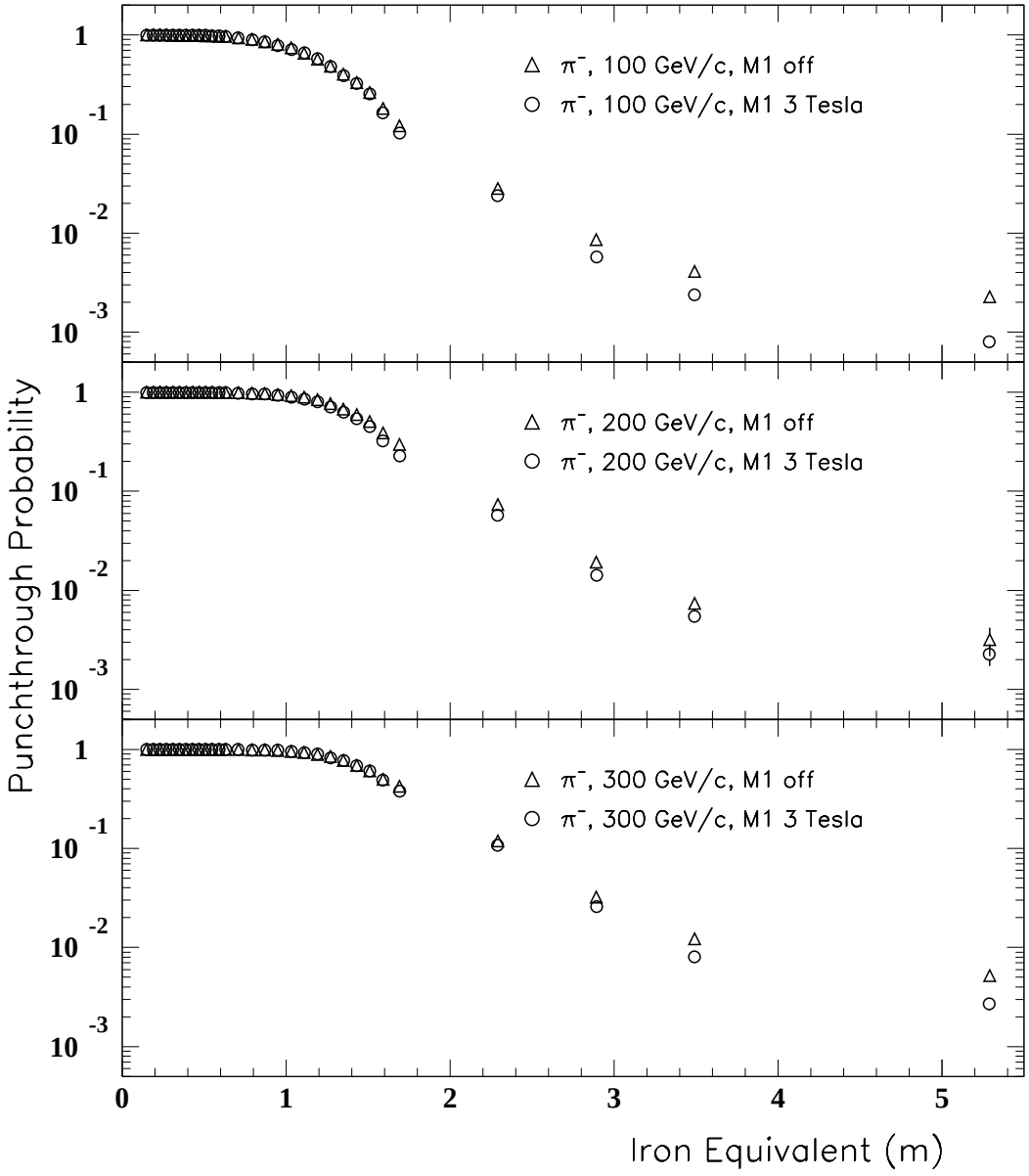

Figure 4: Total punchthrough probability as a function of meters of iron equivalent for 100, 200 and 300 GeV/c negative pions. We compare data taken with the M1 field at 3 T and M1 off.

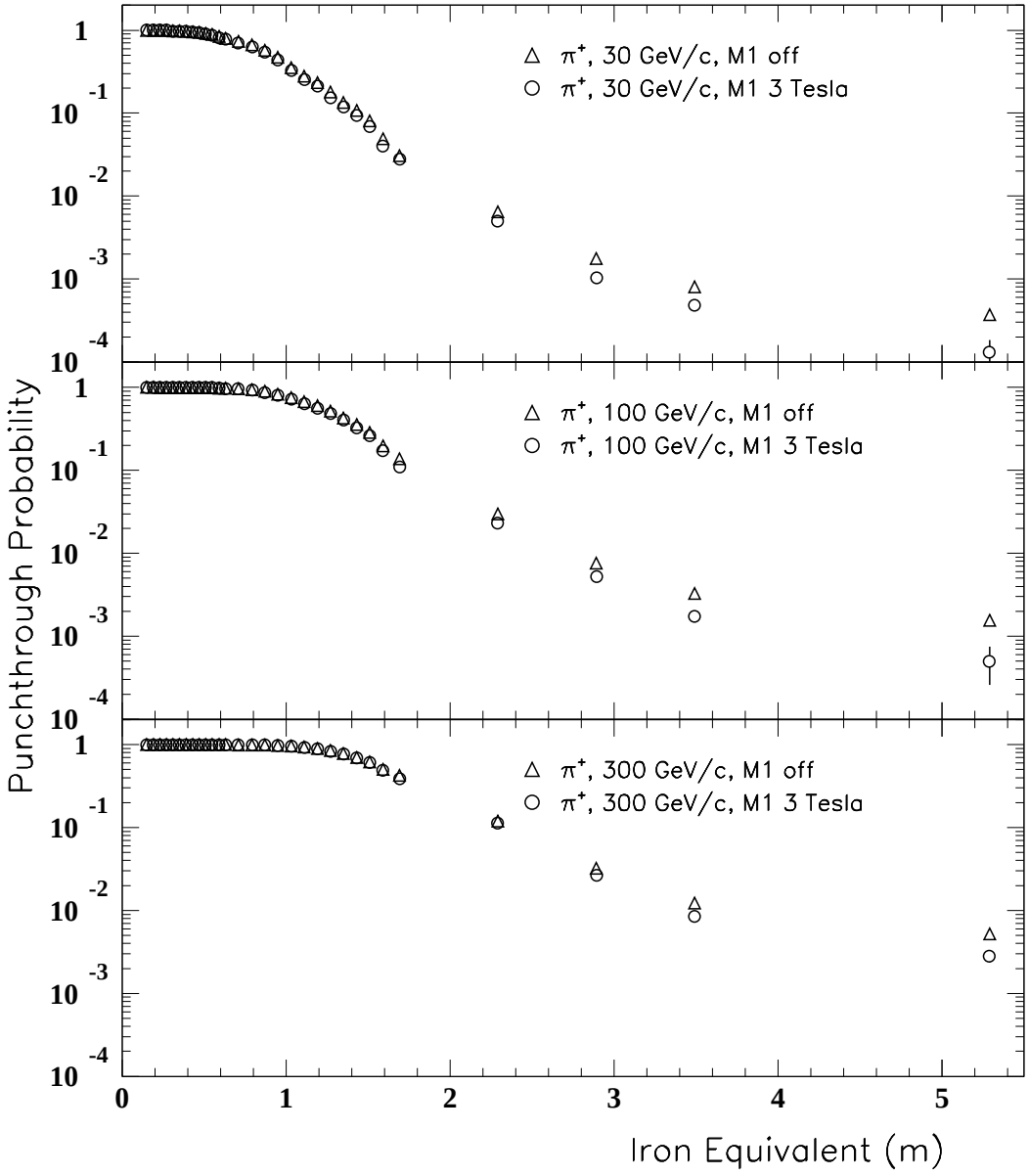

Figure 5: Total punchthrough probability as a function of meters of iron equivalent for 30, 100 and 300 GeV/c positive pions. We compare data taken with the M1 field at 3 T and M1 off.

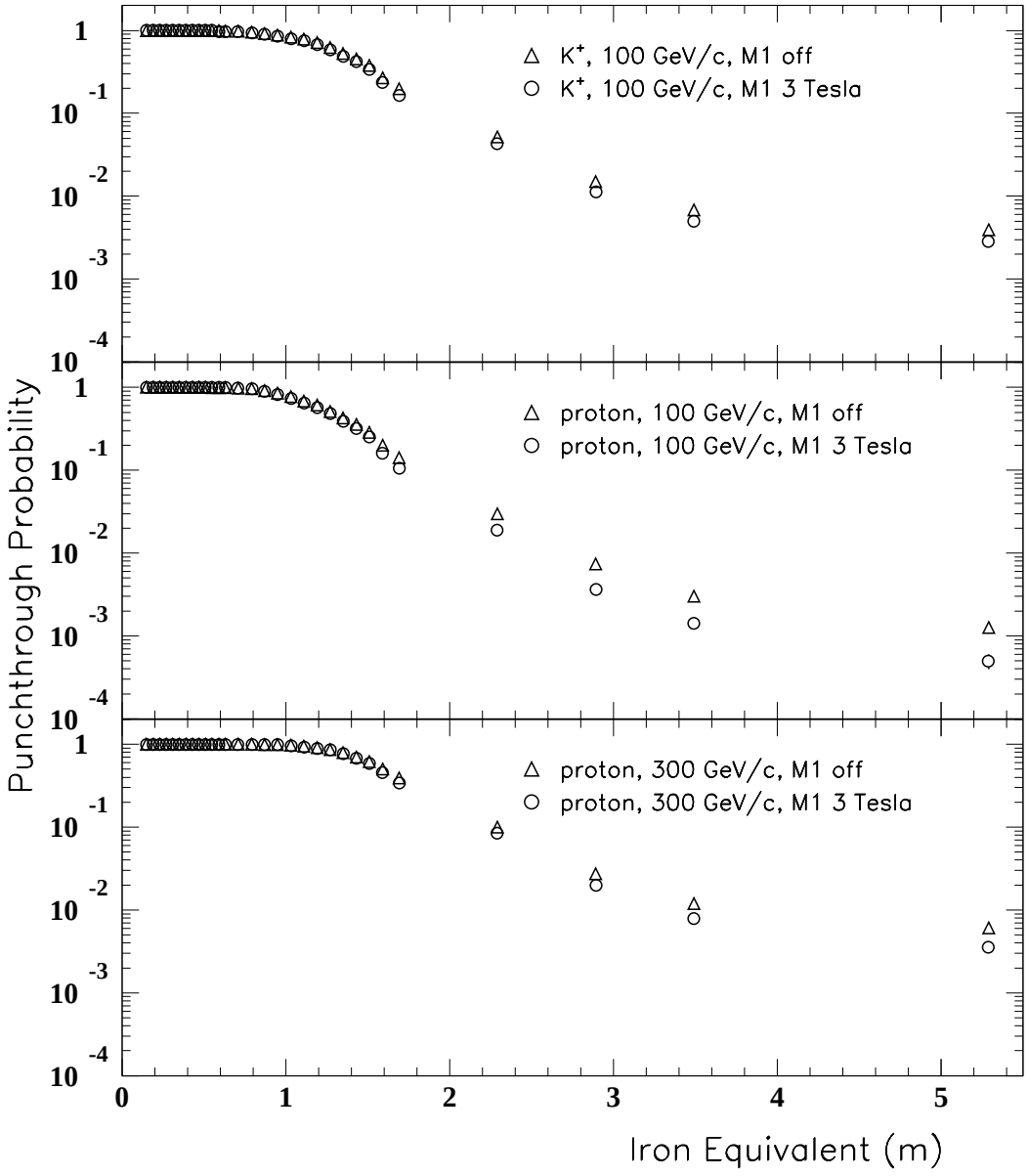

Figure 6: Total punchthrough probability as a function of meters of iron equivalent for 100 GeV/c positive kaons and 100 and 300 GeV/c protons. We compare data taken with the M1 field at 3 T and M1 off.

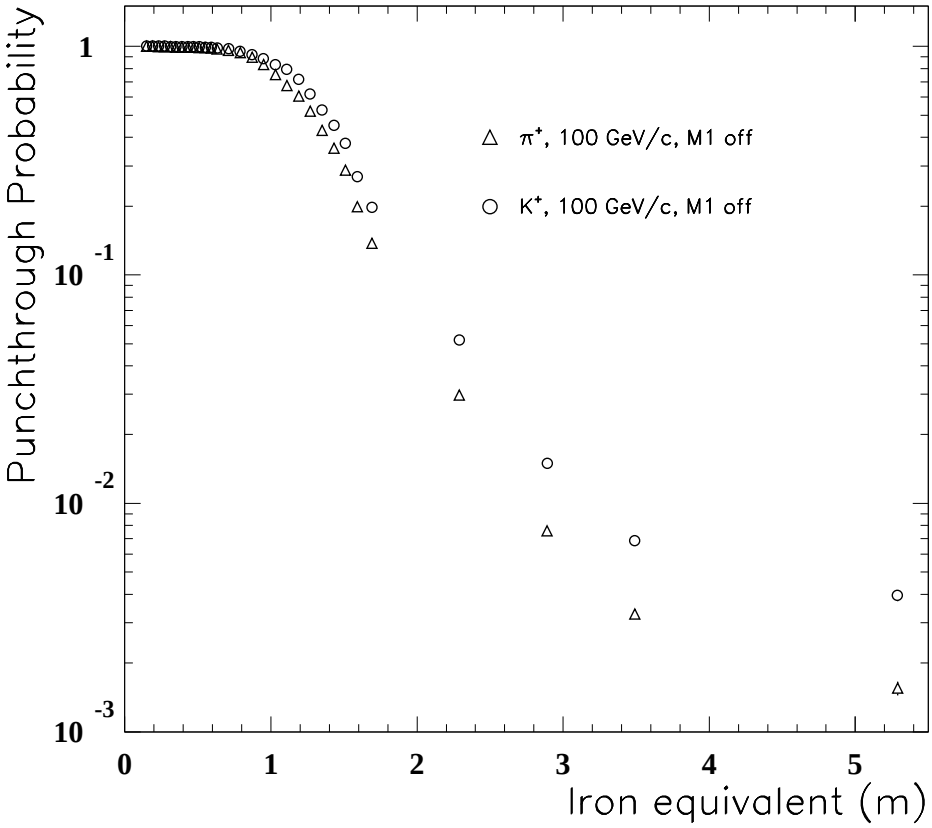

Figure 7: The total punchthrough probability, as a function of meters of iron equivalent, of 100 GeV/*c* positive pions and positive kaons are compared.

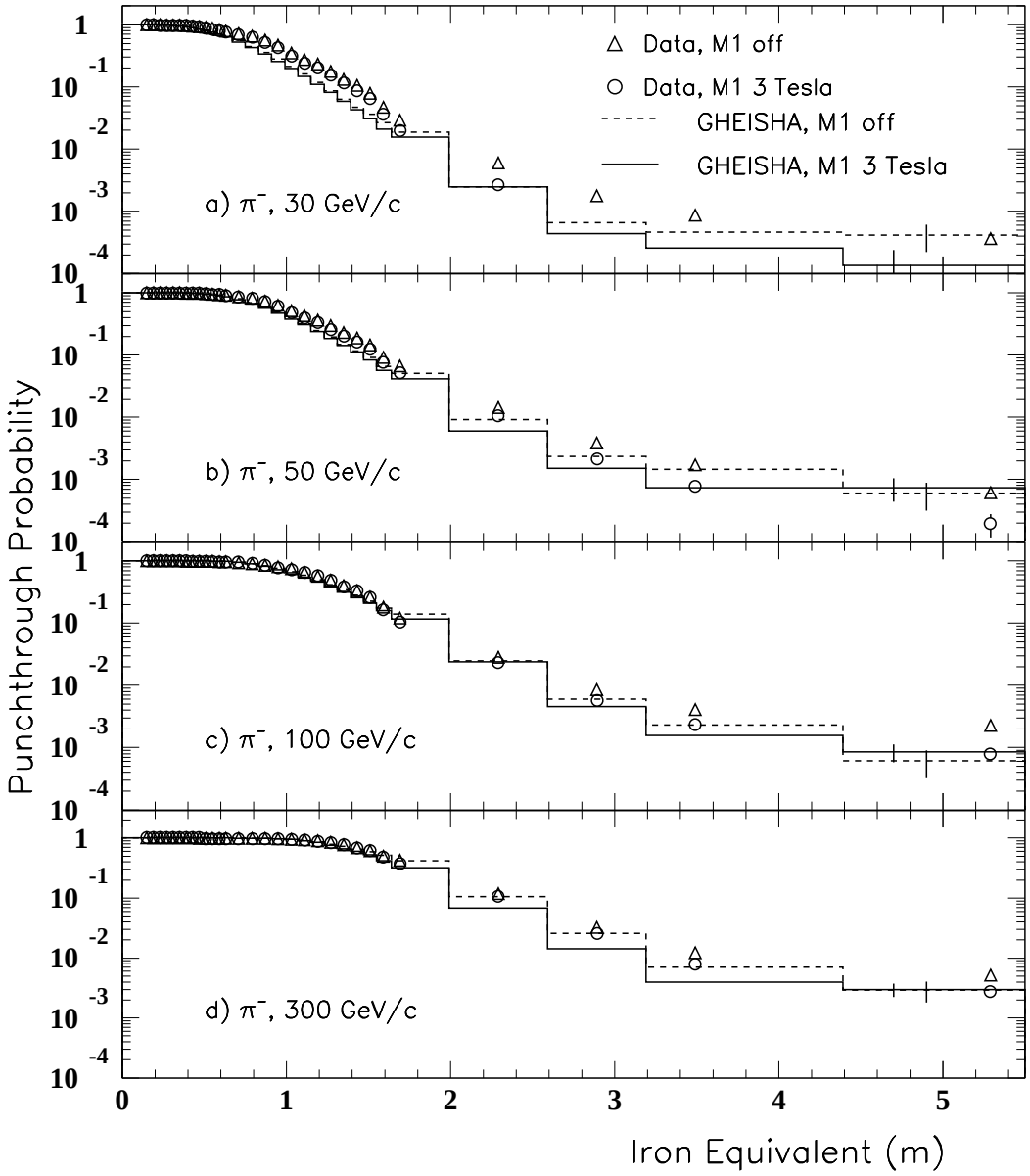

Figure 8: The total punchthrough probability as a function of meters of iron equivalent of 30, 50, 100, and 300 GeV/c simulated negative pions are compared with the results of analysis of real data. Hadronic interactions were simulated using GHEISHA. The statistical error for the simulated data is shown for the last bin.

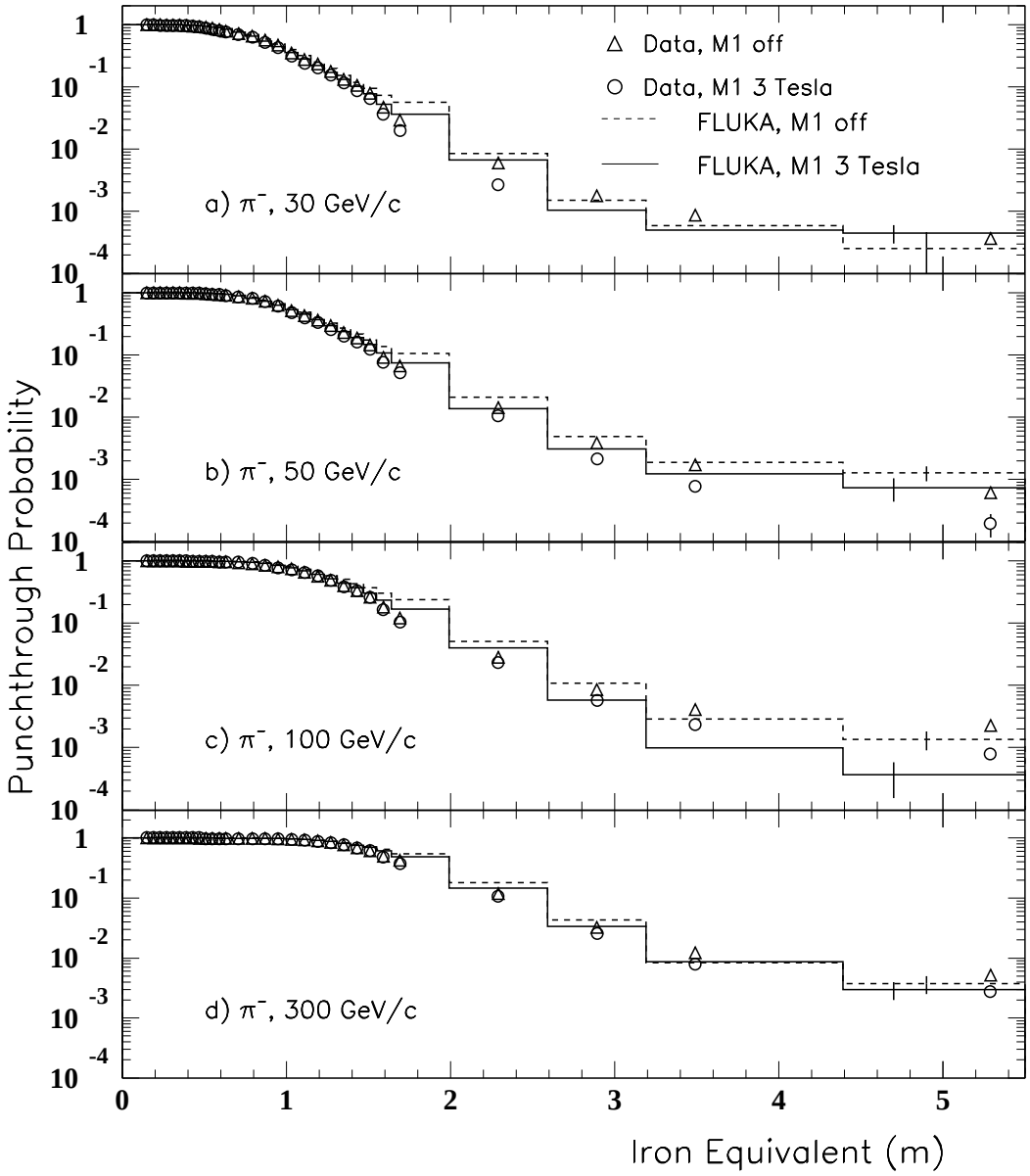

Figure 9: The total punchthrough probability as a function of meters of iron equivalent of 30, 50, 100, and 300 GeV/c of simulated negative pions are compared with the results of analysis of real data. Hadronic interactions were simulated using FLUKA. The statistical error for the simulated data is shown for the last bin.

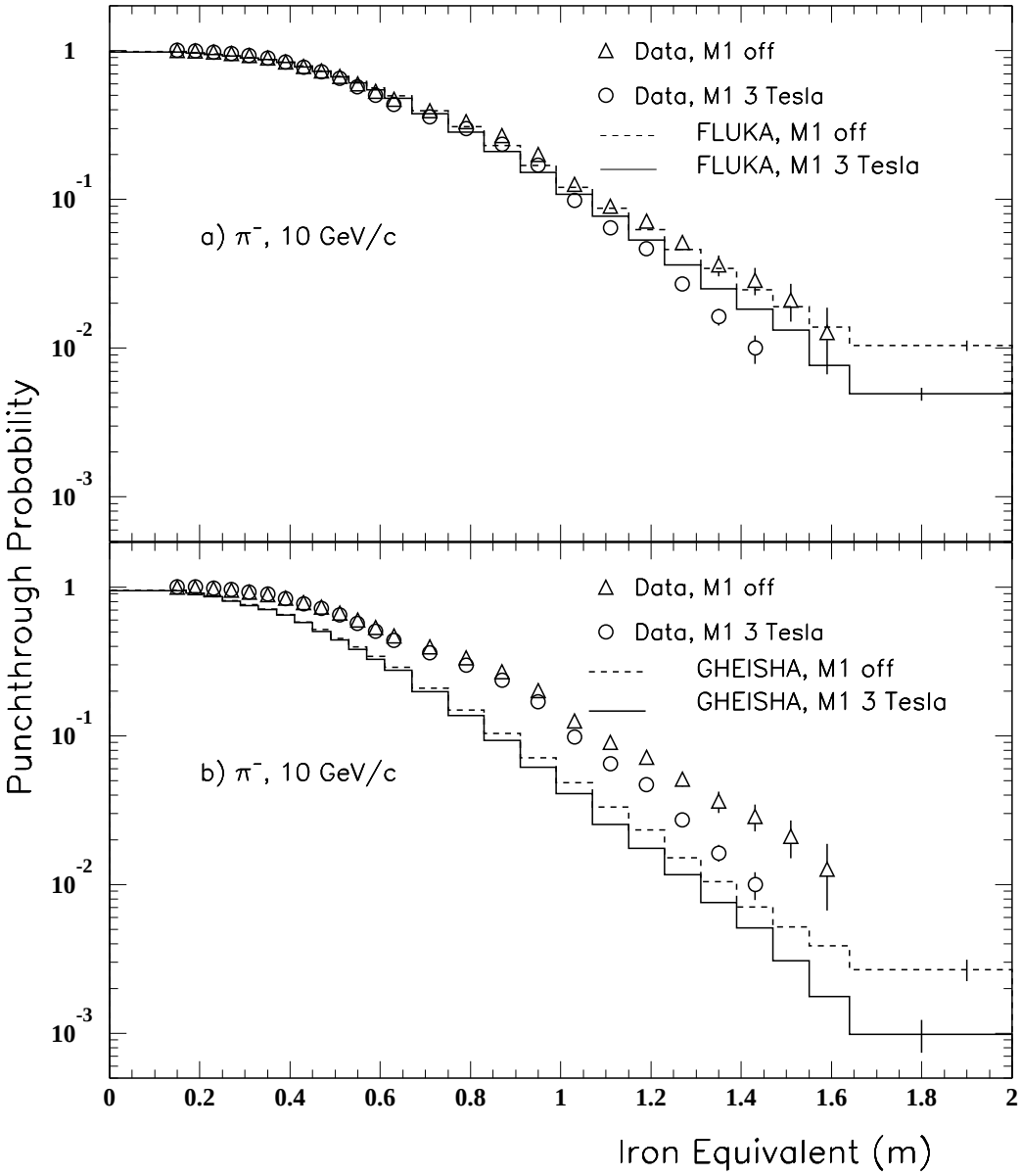

Figure 10: The total punchthrough probability as a function of meters of iron equivalent of 10 GeV/c simulated negative pions is compared with the results of analysis of real data. In a) hadronic interactions were simulated using FLUKA, in b) using GHEISHA. The statistical error for the simulated data is shown for the last bin.

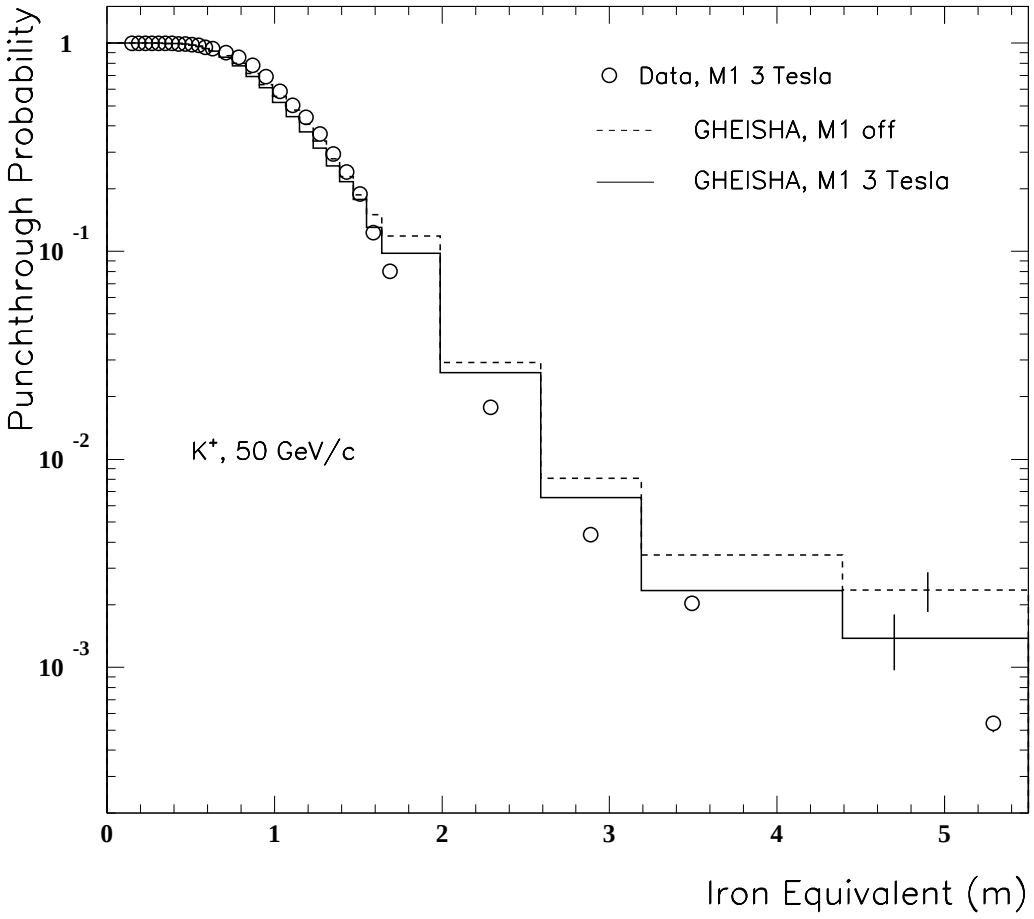

Figure 11: The total punchthrough probability as a function of meters of iron equivalent of 50 GeV/c simulated positive kaons is compared with the results of analysis of real data. Hadronic interactions were simulated using GHEISHA. The statistical error for the simulated data is shown for the last bin.

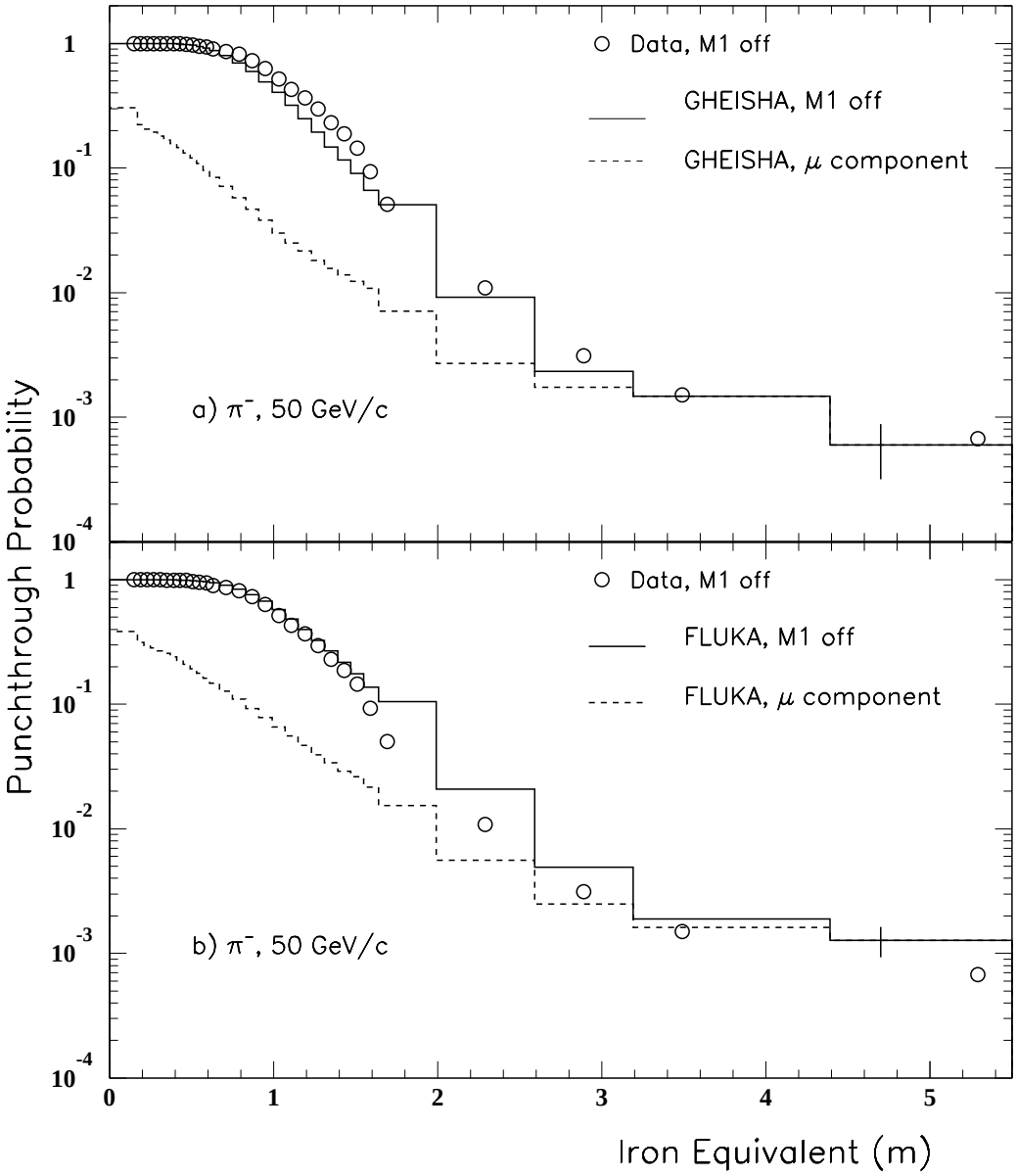

Figure 12: The total punchthrough probability, as a function of meters of iron equivalent, of 50 GeV/c simulated negative pions is plotted as a solid line with the muon component indicated as a dashed line. In a) hadronic interactions were simulated using GHEISHA, in b) using FLUKA. The statistical error is shown for the last bin.

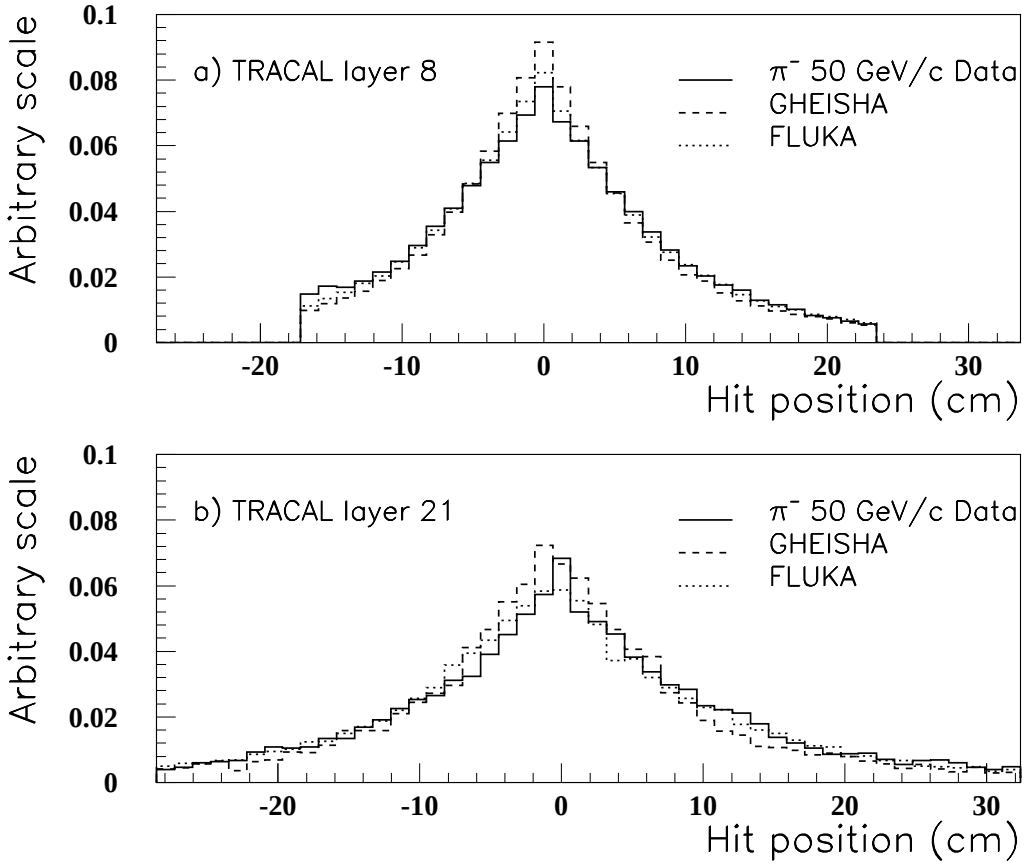

Figure 13: Hit profile of TRACAL wires, for data taken with M1 off, at a) layer 8 ($\approx 2.5\lambda$), and b) layer 21 ($\approx 7.5\lambda$). The real 50 GeV/*c* negative pion data (solid line) is compared with data simulated using GHEISHA (dotted line) and FLUKA (dashed line) to simulate hadronic interactions. The wire pitch is 12.7 mm. The histograms have been normalized by the total number of events.

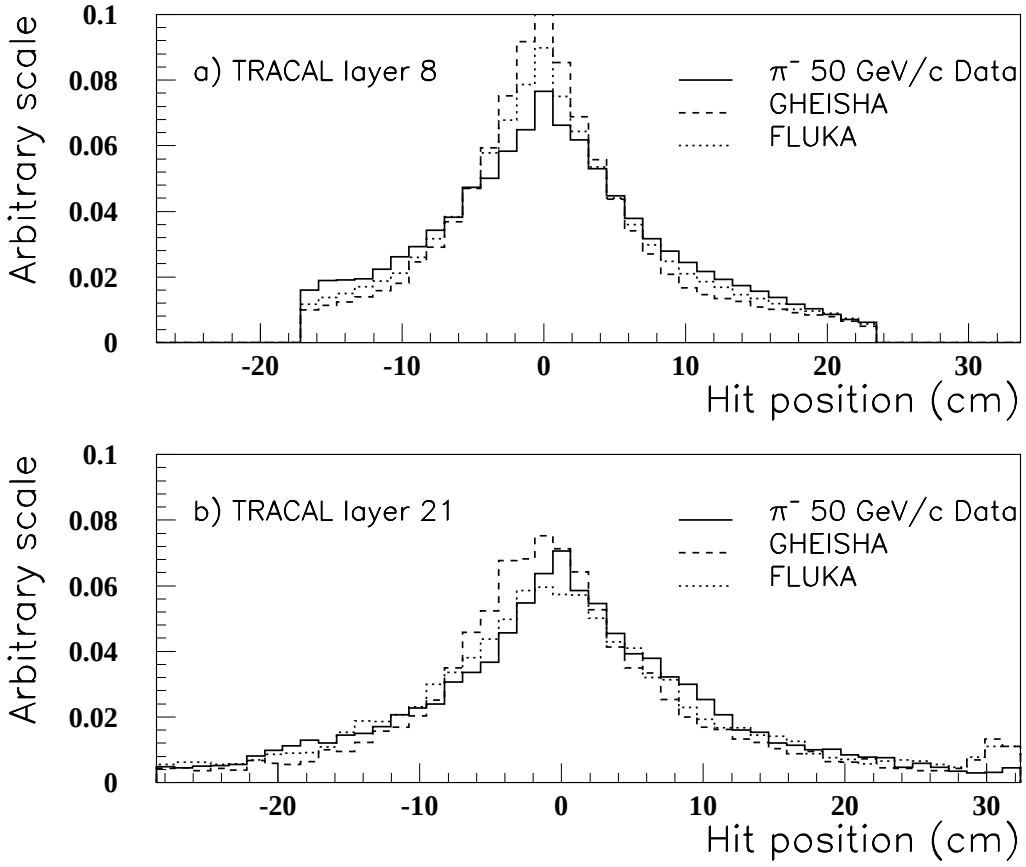

Figure 14: Hit profile of TRACAL wires, for data taken with a M1 of 3 T, at a) layer 8 ($\approx 2.5\lambda$), and b) layer 21 ($\approx 7.5\lambda$). The real 50 GeV/c negative pion data (solid line) is compared with data simulated using GHEISHA (dotted line) and FLUKA (dashed line) to simulate hadronic interactions. The wire pitch is 12.7 mm. The histograms have been normalized by the total number of events.

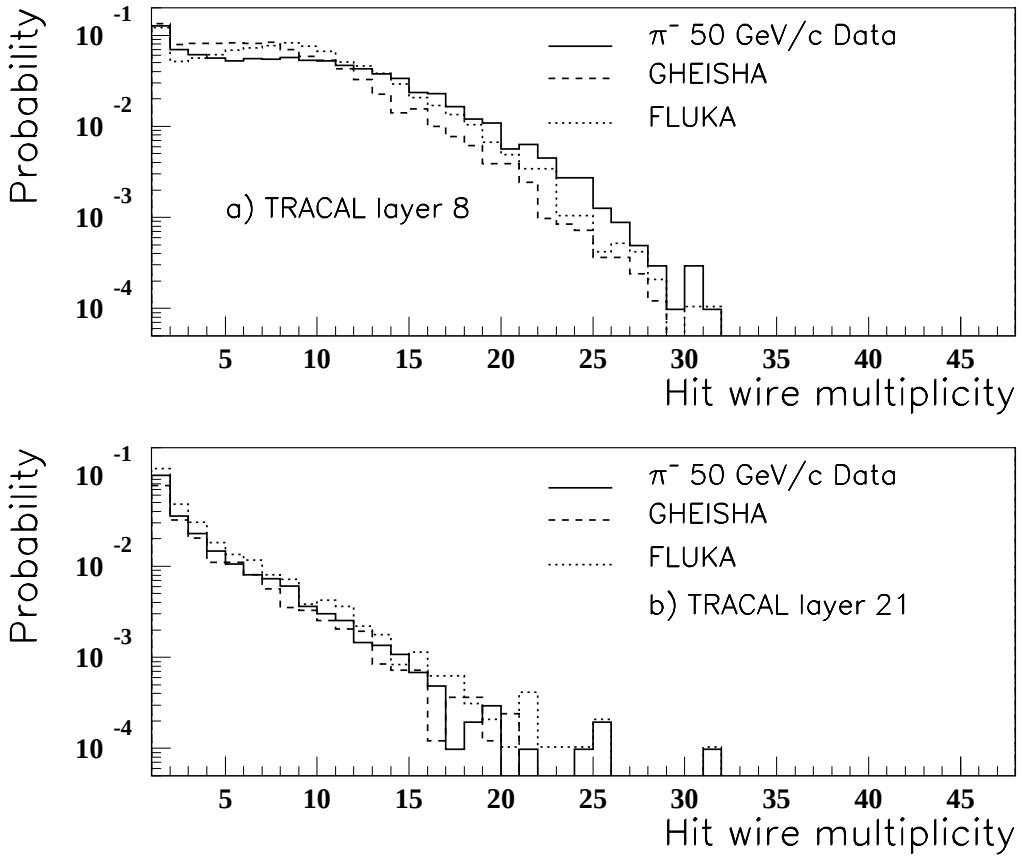

Figure 15: Multiplicity of hit TRACAL wires, for data taken with M1 off, at a) layer 8 ($\approx 2.5\lambda$), and b) layer 21 ($\approx 7.5\lambda$). We compare real 50 GeV/*c* negative pion data (solid line), with data simulated using GHEISHA (dotted line) and FLUKA (dashed line) to simulate hadronic interactions. The number of events with zero multiplicity are not shown. The histograms have been normalized by the total number of events.

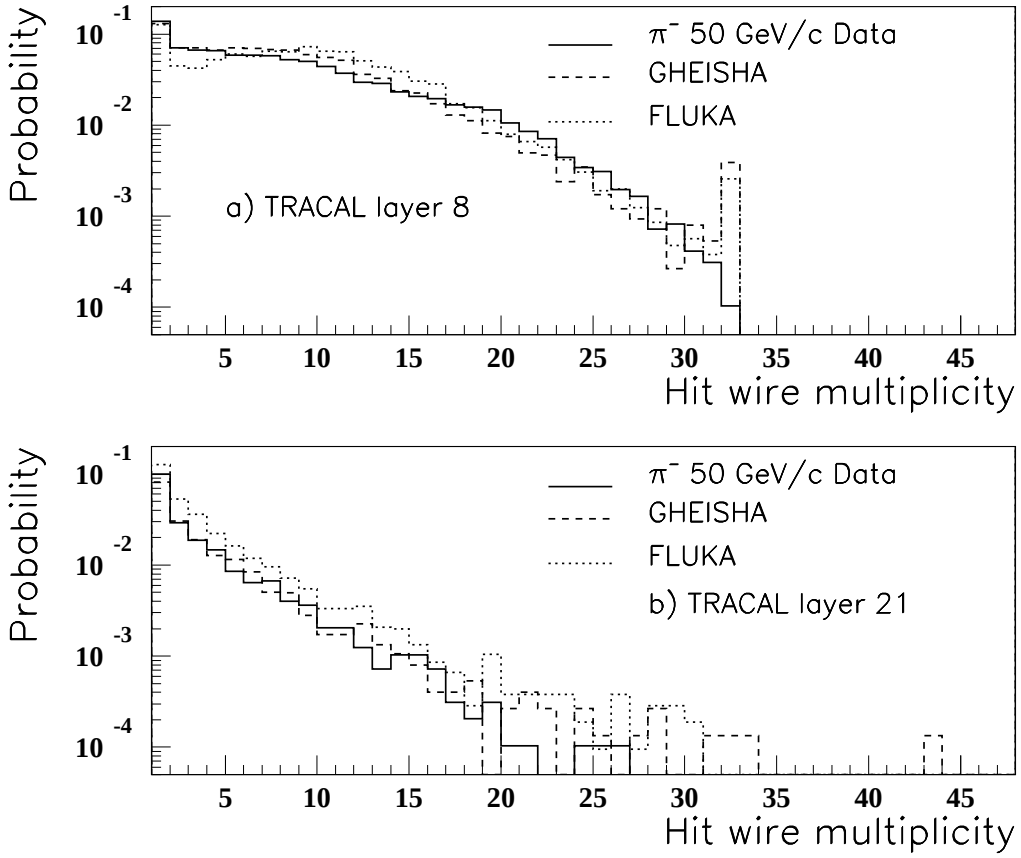

Figure 16: Multiplicity of hit TRACAL wires, for data taken with the field of M1 at 3 T, at a) layer 8 ($\approx 2.5\lambda$), and b) layer 21 ($\approx 7.5\lambda$). We compare real 50 GeV/c negative pion data (solid line), with data simulated using GHEISHA (dotted line) and FLUKA (dashed line) to simulate hadronic interactions. The number of events with zero multiplicity are not shown. The histograms have been normalized by the total number of events.

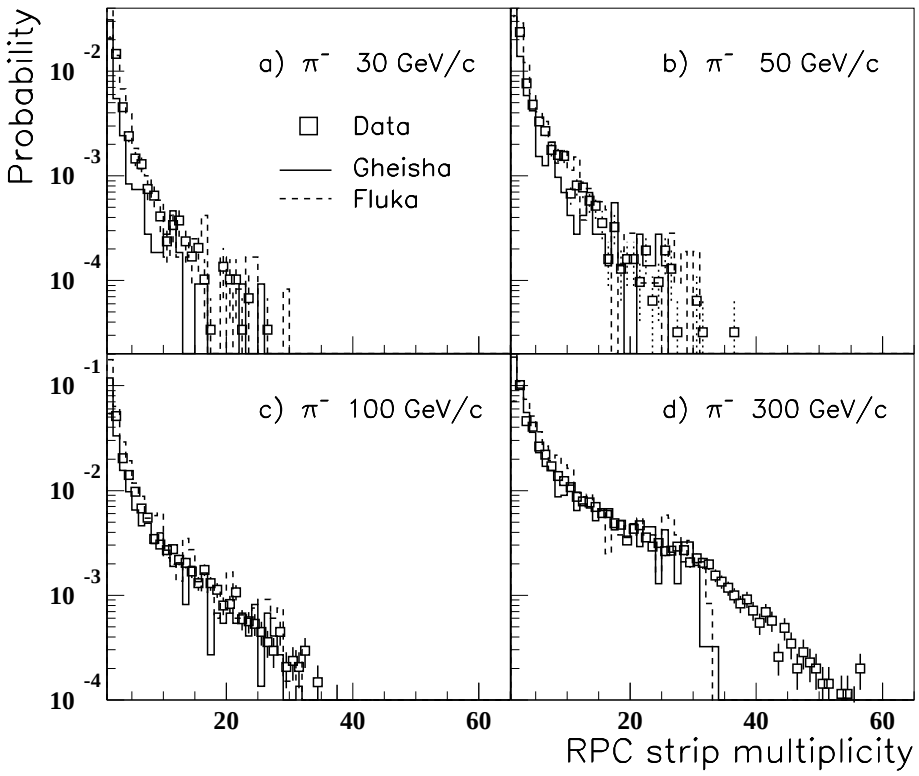

Figure 17: Multiplicity of hit RPC strips in Station 1 ($\approx 10\lambda$) from showers originating from negative pions of momenta a) 30 GeV/c, b) 50 GeV/c, c) 100 GeV/c and d) 300 GeV/c. The data were taken with the magnet M1 off. We compare the results from analysis of real data (open squares) with data simulated using GHEISHA (solid line) and FLUKA (dashed line) to simulate hadronic interactions. The number of events with zero multiplicity are not shown. The histograms have been normalized by the total number of events.

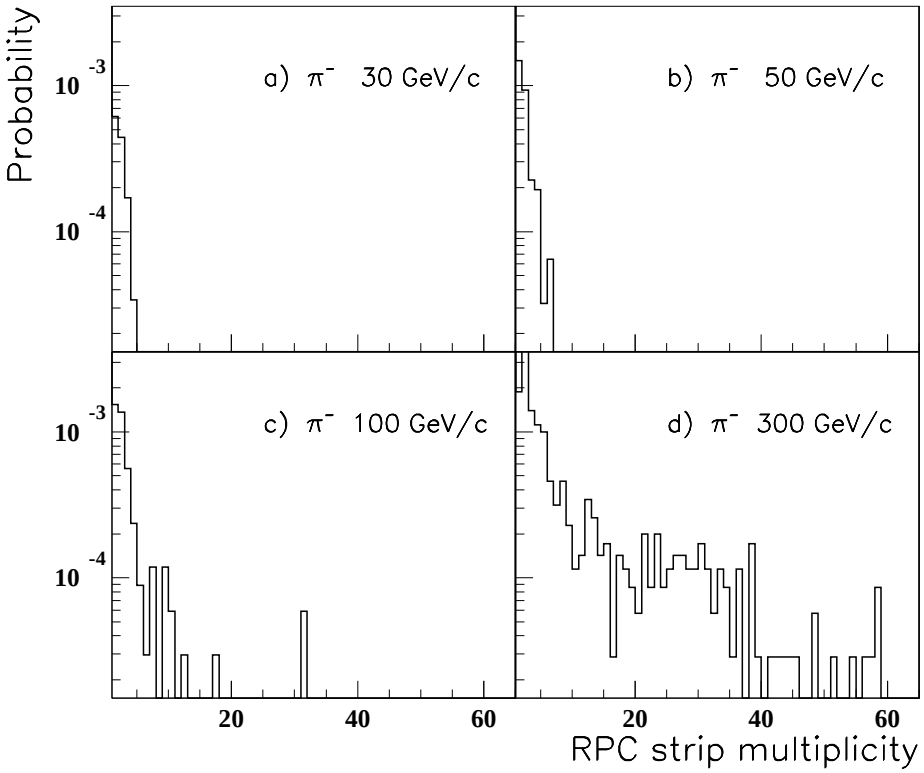

Figure 18: Multiplicity of hit RPC strips in Station 1 ($\approx 10\lambda$) when we require that there is also a hit recorded in Station 2 ($\approx 20\lambda$). The showers originated from negative pions of momenta a) 30 GeV/c, b) 50 GeV/c, c) 100 GeV/c and d) 300 GeV/c when a hit is recorded in Station 2 ($\approx 20\lambda$). The data were taken with the magnet M1 off. The histograms have been normalized by the total number of events.